Research Square

Preprints are preliminary reports that have not undergone peer review.
They should not be considered conclusive, used to inform clinical practice,
or referenced by the media as validated information.

Microphytobenthos primary production and organic matter mineralization along the sea level gradient in a tropical mudflat

Alfonso Corzo

alfonso.corzo@uca.es

Universidad de Cádiz: Universidad de Cadiz https://orcid.org/0000-0003-3718-941X

Eddy Gómez-Rámirez

Universidad de Costa Rica

Emilio García-Robledo

University of Cadiz - Cadiz Campus: Universidad de Cadiz

Sara Haro

CSIC: Consejo Superior de Investigaciones Cientificas

Julio Bohórquez

Universidad de Cádiz Facultad de Ciencias del Mar y Ambientales: Universidad de Cadiz Facultad de Ciencias del Mar y Ambientales

Juan Luis Jiménez-Arias

Universidad de Cadiz Facultad de Ciencias del Mar y Ambientales

Sokratis Papaspyrou

Universidad de Cadiz Facultad de Ciencias del Mar y Ambientales

Research Article

Keywords: benthic microalgae, tidal flat, tropical estuary, sediment oxygen microprofiles, sediment inorganic nutrients, microphytobenthic primary production

Posted Date: June 25th, 2026

DOI: https://doi.org/10.21203/rs.3.rs-10084535/v1

License: This work is licensed under a Creative Commons Attribution 4.0 International License.
Read Full License

Version of Record: A version of this preprint was published at Estuaries and Coasts on October 9th, 2026. See the published version at https://doi.org/10.1007/s12237-026-01823-1.

Microphytobenthos primary production and organic matter mineralization along the sea level gradient in a tropical mudflat

Corzo[1,2]*, Alfonso, Eddy Gómez-Ramírez[1,3], Emilio Garcia-Robledo[1,2], Sara Haro[1,4], Julio Bohórquez-Ferrando[1], Juan Luis Jiménez-Arias[1], Sokratis Papaspyrou[1,2].

[1] Department of Biology, Faculty of Marine and Environmental Sciences, University of Cadiz, 11510, Cadiz, Spain

[2] University Institute of Marine Research (INMAR), Puerto Real Campus, 11510, Cadiz, Spain

[3] Universidad de Costa Rica, Escuela de Química y CIMAR, San Pedro Montes de Oca, 11501-2060, San José, Costa Rica.

[4] Department of Ecology and Coastal Management, Institute of Marine Sciences of Andalusia (ICMAN), Spanish National Research Council (CSIC), 11510, Cadiz, Spain

* corresponding author:

Alfonso Corzo

E-mail: alfonso.corzo@uca.es

ABSTRACT

Tropical tidal flats represent more than half of the global tidal flat area, however information on the ecological and biogeochemical role of MPB in tropical environments remains scarce. MPB spatiotemporal dynamics and sediment biogeochemistry are influenced by physicochemical and biological factors such as emersion time, irradiance, desiccation, and grazing, which vary along the sea-level (SL) gradient in the intertidal zone. Sediment biogeochemistry, MPB biomass, community composition and net metabolism changed along the SL gradient in a tropical tidal flat at Punta Morales, Gulf of Nicoya (Costa Rica). Proportion of fine particles, organic matter, organic carbon, and total nitrogen increased with SL, likely due to higher mangrove inputs and local MPB production, greater deposition of fine particles and higher preservation capacity associated with reduced oxygen penetration and increased surface area of fine particles. Inorganic nutrients were partitioned among porewater, intracellular and exchangeable pools. Ammonium, phosphate, and silicate were mainly associated with intracellular pools, whereas nitrate was primarily present in porewater. MPB biomass, dominated by diatoms, decreased seaward, while cyanobacteria were relatively more abundant at higher SL. MPB photosynthesis enhanced sediment oxygenation and likely stimulated aerobic mineralization landward. Net primary production and respiration increased with SL, being the main predictor of changes across the intertidal. These results increase our knowledge on tropical tidal flats, highlighting the strong ecological and biogeochemical zonation across the intertidal gradient. Considering this zonation is essential for accurately scaling up site-specific measurements and for improving estimates of the contribution of intertidal sediments to the overall carbon and nutrient dynamics of coastal ecosystems.

Key words: benthic microalgae, tidal flat, tropical estuary, sediment oxygen microprofiles, sediment inorganic nutrients, microphytobenthic primary production

Highlights:

- Sediment organic matter, organic carbon and total nitrogen increased with sea level
- MPB abundance, net primary production and respiration increased with sea level
- Diatoms dominate MPB but cyanobacteria proportion increases with sea level
- Ecological and biogeochemical zonation are key factors in tropical intertidal flats

1. Introduction

Coastal zones, though representing a small fraction of the global ocean, hold a disproportionate large ecological and socio-economic importance due to the diversity of habitats they encompass — including mangroves, salt marshes, intertidal mudflats, and subtidal seagrass meadows. Among these, unvegetated intertidal sediments make a major contribution to the overall primary production of shallow coastal systems (Underwood & Kromkamp, 1999; Haro et al., 2020). The high productivity of tidal flats is sustained by the photosynthetic community of benthic microorganisms known as microphytobenthos (MPB), composed mainly of diatoms and cyanobacteria. MPB, in addition to carbon production and storage in intertidal sediments, regulates oxygen and nutrient exchange across the sediment–water interface, thereby influencing local biogeochemical cycles and the mineralization of organic matter (Hope et al., 2020). MPB also excretes a fraction of its photosynthetically fixed carbon as extracellular polymeric substances (EPS), (Hofmann et al., 2009), which enhance sediment stability (Underwood & Paterson, 2003; Ubertini et al., 2015) and constitute an important carbon and energy source for benthic bacteria, and meio- and macrofauna (Middelburg et al., 2000; Bohórquez et al., 2017). So far, most studies on MPB ecological and its biogeochemical roles have been conducted in temperate coastal and estuarine systems (Brito et al., 2013; Haro et al., 2020; Kwon et al., 2020), whereas information from tropical intertidal zones remains scarce (Corzo et al 2024; Haro et al 2025, Benny et al 2021, Oliveira et al 2011, Lin et al., 2020, Salleh & McMinn 2021), even though these environments represent more than half of the global tidal flat areas (Murray et al., 2019). This lack of knowledge is critical since the ecological functioning and biogeochemical

role of MPB in tropical tidal flats might differ substantially from those in temperate regions and represent a large area.

Intertidal sediments are transitional environments exposed to multiple stressors, such as immersion period, irradiance dose, sediment grain size, and water column turbulence, whose relative effect depends on the position of the benthic community along the sea level (SL) range. MPB activity and biomass are largely determined by these factors, as well as biological interactions such as grazing and competition (Underwood and Kromkamp, 1999; Brito et al., 2013; Daggers et al., 2020; Haro et al., 2020; Savelli et al., 2021). Changes in MPB activity along the SL gradient are also likely to affect sediment biogeochemistry. For example, photosynthetic O_2 production by MPB, which is expected to change along SL, strongly influences sediment oxygen availability in the sediment, and therefore the rates and pathways of organic matter mineralization. These, in turn, might determine the magnitude and direction of inorganic nutrient fluxes across the sediment–water interface. Therefore, the main objective of this study is to analyze the distribution of MPB biomass, community composition and net metabolism along the gradient of SL and its effect on sediment biogeochemistry in Punta Morales (inner Golf of Nicoya) as model of estuarine tropical tidal flats.

Tropical regions differ markedly from temperate ones in that they experience consistently high light intensity and temperature throughout the year. In temperate systems, MPB primary production typically follows seasonal patterns, with production peaks in summer or winter depending on latitude, due to differences in the optimal combination of light and temperature during the year (Orvain et al., 2012; García-Robledo et al., 2016). In contrast, in tropical environments irradiance and temperature are more stable year-round which might influence

113 differently the coupling between MPB primary production, biomass, and sediment
114 biogeochemistry. However, little information is available for such tropical intertidal settings.
115 The inner Gulf of Nicoya, located on the Pacific coast of Costa Rica, is a tropical estuary
116 recognized as one of the most productive worldwide (Soria-Píriz et al., 2017, Cloern et al.,
117 2014). Although numerous studies have examined various aspects of its pelagic environment
118 (Palter et al., 2007; Seguro et al., 2015; Soria-Píriz et al., 2017, 2024) and the benthic–pelagic
119 coupling with subtidal aphotic sediments along the estuarine gradient (Gómez-Ramírez et
120 al., 2019), the intertidal sediments of the Gulf have received little scientific attention despite
121 the extensive tidal flats that fringe the inner estuary. Recently Corzo et al (2024) estimated
122 that the total daily average contribution of MPB primary production in tidal flats of inner gulf
123 was comparable to the total input of allochthonous C from the Tempisque River. However,
124 this estimate did not consider the wide variability in MPB biomass and cover among the
125 different tidal flats, and more importantly the systematic changes in biomass and cover across
126 the SL range (Haro et al 2025, Corzo et al 2024). Here we explore specifically the role of SL
127 in shaping the spatial distribution of MPB biomass, net sediment metabolism and the
128 biogeochemical characteristics of the sediment, including the content of organic carbon, total
129 nitrogen and different inorganic nutrients pools within the sediment of tropical estuary.

130 We hypothesized that MPB primary production and the biogeochemical processing of
131 organic matter and inorganic nutrients in tropical intertidal sediments would be considerably
132 affected by SL. To test this, we investigated an unvegetated intertidal mudflat in the inner
133 part of the Gulf of Nicoya (Punta Morales, Costa Rica) with the following objectives: 1) To
134 characterize the MPB biomass, abundance and community compositions and its relationship
135 with physical and chemical sediment properties along the intertidal gradient of SL, 2) To

quantify MPB primary production and net metabolism at different SL to refine future estimations of the contribution of MPB to the overall system productivity and C budget and, 3) To measure organic matter mineralization rates and evaluate the contribution of different inorganic nutrient pools to total sediment content along the SL gradient. These data can help refine available C and N budget for this and other tropical estuaries, improving the knowledge of the global contribution of MPB and tropical tidal flats to earth system net metabolism.

2. Material and methods

2.1. Study site and sampling

The Gulf of Nicoya located at the Pacific coast of Costa Rica (10ºN and 85ºW) is divided in two basins. The shallow (20 m maximum depth) inner basing has estuarine characteristics driven by the Tempisque River (Palter et al 2007; Seguro et al 2015; Soria-Píriz et al 2017) and extends roughly to Punta Arenas (Fig. 1). The area presents a semi-diurnal and mesotidal regime with a mean tidal amplitude of 2.28 m (Módulo de Información Oceanográfica-CIMAR 2012, https://miocimar.ucr.ac.cr/). The high tidal amplitude, the low coastline, and the large sediment input from the riverine discharges produce extensive intertidal unvegetated mudflats surrounded by mangroves in the inner basin.

Samplings were carried out during the dry season of two consecutive years along two transects in the intertidal zone from the mangrove edge (Transect A in April 2012 and Transect B in January 2013) in Punta Morales, on the east coast of the inner basin (Fig. 1). Three sampling points were established along the tidal range in each transect: low, middle and high. Every sampling point was georeferenced, and the sea level (SL) with respect to the

158 local mean sea level (MSL) determined from a digital bathymetry map prepared as described
159 below. At each transect point, 6 sediment cores (15 cm long, 5 cm inner diameter) were
160 collected within one m^2 plot. Three additional sediment cores were collected from every plot
161 in Transect B in 2013 for the determination of total CO_2 production rates. All sediment cores
162 were transported (10 min) to the laboratory at the Estación Nacional de Ciencias Marinas
163 (http://www.ecmar.una.ac.cr/), Universidad Nacional de Costa Rica (UNA). Cores used for
164 microsensor measurements were maintained in an aquarium within *in situ* seawater for
165 acclimation to laboratory conditions (25° C) under an halogen lamp at 150 µmol m^{-2} s^{-1},
166 whereas the remaining cores for sediment variables determinations were kept on ice until
167 further processing during the same day.

168

169 **2.2. Oxygen microprofiles and rates of primary production and dark respiration**

170 Vertical O_2 microprofiles were performed in three of the sediment cores collected at each
171 transect sampling point with oxygen microelectrodes (tip diameter: 50 µm, UNISENSE®) in
172 light (1500 µmol photons m^{-2} s^{-1}, Schott KI-1500) and darkness. The microelectrodes were
173 mounted on a motor-controlled micromanipulator (MC-232; Unisense®) connected to a PC
174 laptop. Microelectrode signal was measured by a high-sensitivity picoammeter (PA2000;
175 Unisense®) and registered in the same laptop via an A/D converter (ACD-816; Unisense®)
176 and using software SensorTracePRO (Unisense®). Oxygen microelectrodes were calibrated
177 using the air-bubbled bulk water phase of the core (100% oxygen saturation) and the
178 sediment anoxic layer (0% saturation). O_2 microprofiles were done with a 100 µm vertical
179 resolution.

Net primary production (P_N) and dark respiration (R_D) rates were determined from the oxygen microprofiles in light and in the dark respectively (Kühl *et al.* 1996, García de Lomas et al. 2005, Corzo et al. 2009). Briefly, oxygen fluxes across the sediment-water interface were calculated using the equation of Fick's first law of diffusion. P_N was estimated as the diffusive flux across the benthic boundary layer (DBL) over sediment surface under light conditions and R_D was estimated as the flux of oxygen into the sediment in dark conditions. P_N and R_D were initially expressed in mmol O_2 m^{-2} h^{-1}. When needed for comparison they were expressed in C units as well using a photosynthetic ratio of 1.2 (Oviatt *et al.,* 1986) and a respiratory coefficient (RQ) of 1.95. This RQ value was obtained as a mean estimate of the RQ measured for the Gulf of Nicoya in the sub-littoral system (Gómez-Ramírez *et al.,* 2019).

2.3. Total CO_2 production rates

Total sediment CO_2 production rates were measured only in Transect B. Three additional cores were collected at each sampling plot (low, middle and high) brought immediately to the laboratory and cut into 3 sections (0-1, 1-3 and 3-5 cm depth). The 3 slices of the same depth were pooled and mixed. Then, this mix was used to fill nine 6 ml Exetainer® vials per every sediment depth layer. Immediately, 3 Exetainers from each depth (time 0) were centrifuged (10000 rpm), the pore water supernatant volume quantified and transferred to another Exetainer, containing 100 µl of saturated $ZnCl_2$ and filled up to 6 ml with Milli-Q water. These pore water samples were stored in the dark at 4º C for later analysis. The remaining were incubated in darkness at room temperature and 3 per each depth layer sacrificed after 8 and 21 days. Porewater was extracted from these samples as described for time 0 samples and both porewater samples were stored as previously described. Dissolved total CO_2 (TCO_2) was measured by a modified version of flow injection analysis method of

204 Hall and Aller (1992). The TCO_2 production rate (μmol CO_2 cm^{-3} d^{-1}) was determined as the
205 increase of CO_2 concentration in the sediment exetainers incubations over time.
206

207 **2.4. Photosynthetic pigments, organic matter, carbon and nitrogen content and**
208 **granulometry**

209 The top half centimeter of 3 cores collected from each plot was sliced and independently
210 homogenized. A portion of each slice was used for the determination of chlorophyll a (Chla)
211 and pheophytin (Pheo), organic matter (OM), organic carbon (OC) and total nitrogen (TN),
212 and inorganic nutrients (described in next section). Photosynthetic pigments were extracted
213 from 0.5 - 1 g of homogenized sediment sample in 100% methanol buffered with $MgCO_3$
214 overnight at 4 °C (Thompson et al. 1999). The extracts were centrifuged at 6000 rpm for 10
215 minutes, and the absorbance of each extract measured spectrophotometrically (UNICAM™
216 UV / Vis). Chla and Phaeo were quantified according to equations by Ritchie (2008) and Stal
217 et al. (1984), respectively. Remaining sediment pellets were dried at 60 ºC for 24 h and the
218 pigment concentrations were normalized to the weight of dried sediment. Organic matter
219 content was determined by the loss of ignition method on dried sediment (Heiri et al. 2001).
220 Total carbon, inorganic carbon and total nitrogen contents were quantified by the analysis of
221 precombusted and untreated samples using a LECO CHNS 932® Elemental Analyzer.
222 Organic carbon was determined as the difference between precombusted (inorganic carbon,
223 550 ºC) and untreated (total carbon) samples.

224 Sediment grain size distribution was measured in the upper 5 cm of the 3 sediment cores used
225 for the determination of oxygen microprofiles, once these measurements were finished and
226 subsamples for MPB abundance had been collected (see below). The percentage of fines (<63

mm) was determined by wet sieving after removing organic matter with hydrogen peroxide (H_2O_2) and dispersing the sediment with sodium hexametaphosphate $(NaPO_3)_6$ (Buchanan, 1984). Sediment wet density was determined as the fresh weight of a known volume. Porosity was determined as the loss of water of the same known volume of sediment sample after drying at 60 ºC for 72 h.

2.5 MPB abundance

MPB abundance was determined in the same cores used for the measurement O_2 microprofiles (2-3 h after collection). Once the O_2 microprofiling had finished, the same cores were subcored with a cut syringe (diameter = 2.5 cm) and the first 5 mm were fixed with 2.0 mL of glutaraldehyde (2.25% final concentration, diluted in 5 µm filtered seawater) and stored in the dark at 4 ºC until analysis. The abundance of diatoms and cyanobacteria was determined by taking 20 µl of a diluted (10×) and homogenized sediment suspension. The final abundance corresponded to the mean of 8 counts per sample of the outer squares (1 mm^2) of a Neubauer chamber placed on a Zeiss® Axioskop 2 MOT Plus microscope (model HBO100N).

2.6. Determination of inorganic nutrient content in the pore water, intracellular and exchangeable pools

Phosphate, nitrate, nitrite, ammonium and dissolved silica (DSi) contents in the pore water (PW), intracellular (IC) and exchangeable (EX) pools were measured as follow in a fraction of homogenized subsamples according to García-Robledo et al. (2014, 2016). In brief, a

249 portion of sediment (0.5 g) was centrifuged at 6000 rpm for 10 minutes at 4 °C. The
250 supernatant was collected and stored for the determination of inorganic nutrient in the PW
251 pool. The sediment pellet was resuspended in 4 ml artificial sea water with the same salinity
252 as *in situ* and freeze-thawed 3 times to ensure the breakdown of cells and the release of
253 intracellular content. These freeze-thawed extracts were centrifuged and the supernatants
254 collected and stored for the determination of IC inorganic nutrient contents. To extract the
255 exchangeable nutrient pool, 2 ml of 2M KCl were added to the sediment pellets after the
256 complete elimination of any supernatant, resuspended, and incubated at 4 ºC for 30 min.
257 These suspensions were then centrifuged and the supernatants collected and stored for
258 determination of inorganic nutrient content in the EX pool later. The concentrations of
259 inorganic nutrients in the different pools were determined spectrophotometrically (Grasshoff
260 et al., 1983, García-Robledo et al. 2014) on a microplate reader (BIO TEK™ Power Wave
261 340). All standard solutions were prepared with artificial seawater with the same salinity as
262 that of the samples.
263
264 **2.7. Cartography of the intertidal area**

265 The methodology for determining the inter-tidal bottom heights relative to the local mean
266 sea-level (MSL) in Nicoya Bay was similar to that described by Bishop-Taylor et al. (2018).
267 It is based on the determination of the waterline from satellite multispectral Sentinel-2 images
268 (ESA, scihub.copernicus.eu), by use of the Normalized Difference Water Index (*NDWI*),
269 computed from the green and near-infrared bands (B3 and B8, respectively) as *NDWI* = (B3
270 - B8)/(B3 + B8) (McFeeters, 1996). 170 Sentinel-2A and 2B images, from January 2020 to
271 March 2021, were processed and combined to contemplate the entire study area with a spatial

resolution of 10 m. The water level height respect to MSL at each time was provided by 5-minutes tide-gauge measures at Puntarenas (N 9° 58', E -84° 50'), and the time-spatial tidal phase-lags were inferred from the University of Denmark DTU10 global ocean tide model (Cheng and Andersen, 2011). The inter-tidal bottom heights contemplated by the processed Sentinel-2 images ranged from -1.8 to +1.2 m above MSL, so the maximum inter-tidal range (about ±2 m above MSL) was completed by interpolating data from the 10 m-resolution digital elevation model (DEM) of the Instituto Geográfico Nacional of Costa Rica (www.snitcr.go.cr) for the upper areas, and the GEBCO_2020 0.25°-resolution bathymetry (www.gebco.net) for the lower ones, after referring them to MSL. The final 10 m-resolution grid was projected into WGS84 UTM 16N coordinate system, covering an area of approximately 73 × 75 km.

2.8. Statistical analysis

The differences between stations were studied using an analysis of variance (one-way ANOVA), followed by a post-hoc analysis (Tukey's honestly significant differences). Statistical analyses were done using Past™ and R software. In order to investigate which combinations of environmental variables might explain variations in biomass (Chla), microphytobenthic primary production in light (PN), or sediment dark respiration (Rd), a distance-based multivariate linear model (Dist-LM) was used. Variables considered for the model included Chl (for rates), distance from the shore, sea level, grain size <63 µm, organic carbon (OC), total nitrogen (TN), C:N ratio, pore water nutrients (NH_4^+, NO_2^- , NO_3^--, PO_4^{3-} , DSi), and MPB variables. Collinearity was assessed with a threshold of >|0.8|; TN was correlated with OC, porewater NO_2^- with PO_4^{3-}, and MPB variables with SL. Only the latter

295 in each case was maintained. Visual inspections indicated no need for transformation.
296 Marginal tests were conducted for individual variables, and the BEST procedure was applied
297 for variable selection, using the Second Order Akaike Information Criterion (AICc) for
298 model selection. All analyses were performed with the PRIMER 6 +PERMANOVA software
299 package.

300

301 **3. RESULTS**

302 **3.1. Transect topography, granulometry, organic carbon and total nitrogen**

303 Transect A and B covered a range of sea levels (SL), from 0 m (Transect A) to -1.13 m
304 (Transect B), and presented different slopes, transect B being in a steeper shoreline that
305 transect A (Fig. 1). Differences of sediment grain size were evident along the intertidal
306 transect, with the finest fraction (<63 μm) ranging between 62.2 - 99.2 %, being highest in
307 the upper intertidal, close to the mangrove canopy (Fig. 2A, Table 1). Despite differences
308 among transects there was a clear positive linear relationship between % of fine sediment
309 fraction and SL (r^2= 0.48, $p<0.05$, n= 18). Organic matter content (OM) ranged between 23.8
310 and 54.1 mg cm^{-2} (or 112.4 – 169.1 mg g^{-1}) in transects A and B and increased clearly with
311 SL (r^2= 0.46, $p<0.05$, n= 18). Organic carbon (OC) ranged between 5.4 to 11.6 mg cm^{-2} (25.6
312 - 36.2 mg C g^{-1}) and total nitrogen (TN) between 0.49 to 1.06 mg cm^{-2} (2.3 – 3.5 mg N g^{-1})
313 and as expected were linearly correlated (r^2=0.71, $p<0.05$, n=18). Both increased with SL,
314 although it was only statistically clear in the case of TN (Fig. 2). In contrast, OC:TN (11.5 -
315 17.5) tended to increase seaward due to a stronger decrease of TN with respect to OC (Fig.
316 2). OC:TN correlated significantly with distance to the mangrove fringe (r^2=0.36, $p<0.05$,
317 n=18) and inversely with % of fine sediment (r^2=0.33, $p<0.05$, n=18).

3.2. Inorganic nutrients

The concentrations of inorganic nutrients (NH_4^+, NO_2^-, NO_3^-, PO_4^{3-}, Dissolved Si) in the three sediment pools (PW, IC and EX) varied both in order of magnitude and in relative contributions (Table 2). The most abundant nutrients were NH_4^+ and DSi, 200.7 ± 39.1 and 170.2 ± 57.5 nmol cm^{-2} respectively, and in both cases the IC pool dominated the total nutrient content, 75 and 62 % respectively. Total nutrient content of PO_4^{3-} and NO_3^- were similar, 16.8 ± 6.4 and 16.7 ± 13.7 nmol cm^{-2}, respectively, and one order of magnitude lower. NO_3^- was most abundant in the PW pool (67.6%), whereas PO_4^{3-} was highest in the IC pool (88.1 %), and below detection limit in the EX pool. Total NO_2^- concentration was very low (5.4 ± 3.1), with 83 % of the total in the EX pool(Table 2).

Total NH_4^+ and NO_2^- increased significantly with SL (r^2=0.36, $p<0.05$, n=18) as did their main pools in the sediment, NH_4^+-IC and NO_2^--EX (Fig. 3). Neither total NO_3^- nor any other NO_3^- pools correlated clearly with SL. PO_4^{3-}-IC presented an inverse trend to SL, increasing significantly seaward (r^2=0.40, $p<0.05$, n=18). DSi-IC and DSi-EX decreased with SL (r^2=0.41, $p<0.05$, n=18), while DSi-PW presented a positive relationship with SL, increasing landward (r^2=0.42, $p<0.05$, n=18) (Fig. 3).

The concentrations of most inorganic nutrients in the different pools did not correlate significantly with basic biogeochemical features of the sediments like % fine sediment particles, OM, OC and TN contents (Fig. S1). Exceptions to this general trend were NO_3^- and DSi in the PW pool and NH_4^+-IC which correlated positively with % fine sediment particles, OM, OC and TN contents. Negative correlations were observed between NO_3^- and DSi in the EX pool and the same set of basic sediment characteristics (Fig. S1). The degree of

341 covariance between the inorganic nutrients in the different sediment pools was scarce, only
342 26.3 % of all possible correlations among them were statistically significant which suggest
343 differences in their biogeochemical dynamics (Fig. S1).
344
345 **3.3. Photosynthetic pigments and microphytobenthos abundance**
346 Chlorophyll a (Chla) content ranged between 1.8 to 17.1 μg cm^{-2} and decreased clearly
347 seaward (r^2=0.39, p<0.05, n=18) (Fig. 4). Pheophytin (Pheo) ranged between 4.5 and 26.9
348 μg cm^{-2} and it did not change with SL (result not shown). The Chla:Pheo ratio which can be
349 used as proxy of active chlorophyll decreased clearly seaward (r^2=0.71, p<0.05, n=18).

350 The cell abundance of microphytobenthos in Punta Morales tidal flats was 0.14 - 1.6 $x10^6$
351 cells cm^{-3} (0.6 ± 0.5 $x10^6$ cell cm^{-3} for both transects) (Table 1). MPB abundance decreased
352 statistically clearly seaward (r^2=0.78, p<0.05, n=18) (Fig. 4) and was higher in Transect A
353 than in Transect B (ANOVA, p <0.05), likely due to a higher values of SL in transect A.
354 MPB abundance significantly correlated with Chla (r^2=0.49, p<0.05, n=18) but not with
355 Pheo. In addition, there was a clear positive correlation between MPB and the Chla/Pheo
356 ratio (r^2=0.71, p<0.05, n=18), which supports the use of Chla:Pheo as proxy of MPB Chla.
357 The abundance of MPB showed a positive linear correlation with NH_4^+ in the PW and IC
358 pools, and with DSi and NO_3^- in the PW pool (Fig. S1). The MPB community in the intertidal
359 sediments of Punta Morales was mainly comprised of pennate diatoms (47-81 %) and
360 cyanobacteria (12-52 %), being diatoms generally more abundant particularly in transect B
361 (Table 1). The % of diatoms decreased significantly with SL (Fig. 4d).
362
363 **3.4. Microphytobenthos primary production and community respiration**

364 The clear differences between O_2 microprofiles in dark and light show the important
365 photosynthetic activity of MPB in Punta Morales tidal flats (Fig. 5). In darkness, O_2 was
366 quickly consumed within 1.1 to 2.4 mm (z_{ox}), whereas in light a subsurface O_2 peak was
367 recorded with z_{ox} increasing up to 2.8 mm. MPB net primary production (P_N) and community
368 respiration rates (R_D), calculated from the O_2 profiles in light and in dark respectively, were
369 between 0.5 to 5.8 mmol O_2 m^{-2} h^{-1} and 0.6 to 2.7 mmol O_2 m^{-2} h^{-1}, respectively. P_N and R_D
370 clearly correlated with SL (r^2=0.40-0.43, $p<0.05$, n=17), decreasing seaward (Fig. 6). P_N
371 significantly correlated with RD (r^2=0.33, $p<0.05$, n=17) and with the abundance of diatoms,
372 cyanobacteria, and MPB (r^2=0.54, $p<0.05$, n=17). R_D was positively and clearly correlated
373 with MPB abundance as well, with % of fine sediment particles and NH_4^+-IC, but
374 surprisingly not with the content of OM, OC or TN of the sediment (Fig. S1).
375
376 **3.5. Total CO_2 production rates**

377 The mineralization of organic matter was measured as TCO_2 produced during long term
378 incubation at three different depths and in three SL positions in Transect B (Fig. 7A).
379 Volumetric mineralization rates ranged between 0.2 and 0.9 µmol CO_2 cm^{-3} d^{-1} and they
380 showed no clear changes with sediment depth up to 4 cm (ANOVA $p > 0.05$). Our results
381 showed consistent differences between volumetric and depth-integrated TCO_2 production
382 rates, (areal rates) being highest at the upper SL (Fig. 7B), but differences were not
383 statistically significant (ANOVA $p > 0.05$), likely due to large dispersion of some data.
384
385 **3.6 Multidimensional analysis**

To determine the environmental variables that would better explain the variability of sediment metabolism and MPB biomass, we applied a distance-based multivariate linear modeling (DistLM) on the benthic metabolism (PN and Rd) and Chla data as response variables. Marginal test results showed that 40% of the variation in all three variables could be explained by SL. % Diatom contributed between 21-35%. The % fines could explain approx 25% for Rd and Chla. Finally, Chla could explain 27% only for Rd (Table S1).

The most parsimonious models selected (overall best solutions) included between one and three variables (Table S2). Most of these models included SL, or a combination with other variables such as porewater nutrients. For Chla, most of the model explained more variation by a combination of % fines and porewater nutrients (Table S2).

4. Discussion

4.1. Biogeochemical characteristics of the sediment across the intertidal

Estuarine environments are highly dynamic systems, characterized by strong spatial and temporal variability in abiotic factors along the river–sea gradient. This longitudinal gradient interacts with a transversal gradient across the sedimentary littoral zone. The physicochemical forcing on the sediment surface across the littoral zone is widely dependent on the heigh of the sediment respect to mean sea level. Our results highlight the key role of the SL gradient on the ecological and biogeochemical zonation across tropical intertidal environments and their similarities with temperate systems.

Sea level range and shoreline slope were different in Transects A and B, with the latter exhibiting a steeper SL gradient (Fig. 1, Table 1). This topographic variability seems to explain the spatial heterogeneity in sediment grain size distribution as well (Fig. 2). Fine

409 sediment percentage increased with SL (Fig. 2), consistent with stronger hydrodynamic
410 forcing seaward leading to coarser grains in lower intertidal zones and lower energy in upper
411 intertidal areas accumulating finer sediments (Friedrichs, 2011). The clear correlation
412 between % fine sediment and SL observed in Punta Morales tidal flat occurred in other tidal
413 flats in the Gulf of Nicoya (Corzo et al 2024). In addition to the evident role of SL in the
414 distribution of sediment grain size across the intertidal, there were clear local differences in
415 the sediment grain size among different tidal flats in the inner Gulf of Nicoya (Corzo et al
416 2024). These differences among tidal flats likely depend on local geomorphologic and
417 hydrodynamic conditions, being fine sediment content in the Punta Morales tidal flats in the
418 upper range of fine sediment content in other tidal flats from inner Gulf of Nicoya (Corzo et
419 al., 2024). Sediment grain size is well known to largely affect the content of OM, OC and
420 TN in sediments (Mayer, 1999). Fines sediments showed a higher preservation of OM likely
421 due to a higher relative surface area and sorption capacity, enhancing OM preservation
422 (Hedges & Keil, 1995; Keil et al., 1997) and by reducing aerobic mineralization rates due to
423 lower oxygen penetration within the sediment (Glud, 2008). Accordingly, all three variables,
424 OM, OC and TN, increased with SL, following the fines distribution. OM, OC and TN
425 contents were similar to those reported from other tropical and temperate tidal flats (Corzo
426 et al., 2024; Haro et al 2020; Kristensen et al., 2008; Sanders et al., 2010; Tang et al., 2023;
427 Zou et al., 2023). However, although OC increased with SL, only OM and TN showed a
428 statistically clear correlation with SL in Punta Morales tidal flat (Fig 2). In this aspect, Punta
429 Morales tidal flat differed from the general trend observed for another 14 different tidal flats
430 in the Gulf of Nicoya, where OC covariated clearly with SL (Corzo et al 2024).

The mean OC:TN ratio was 13.2 ± 1.35, similar to those observed in another tidal flats in the area (Corzo et al 2024) and elsewhere (Haro et al 2020; Kristensen et al., 2008; Sanders et al., 2010; Tang et al., 2023; Zou et al., 2023). OC:TN in Punta Morales did not change clearly with SL (Fig. 2), nor in other tidal flats in the gulf (Corzo et al 2024). OC:TN ratios above 10 suggest that both MPB (autochthonous) and mangrove OM (allochthonous) contribute to sedimentary C and N stocks in the area (Hedges et al., 1997; Hillebrand & Sommer, 1999; Corzo et al., 2024). In addition, high OC:Chla ratios (>1000) compared to typical MPB values (10–154, de Jonge 1980) further support an important allochthonous contribution to the organic to OM in the intertidal sediments. In addition, the observed inverse relationship between OC:TN ratio and fine sediment content ($r^2 = 0.33$, $p < 0.05$, n=18) suggests that fine-grained sediments might preferentially adsorb N-rich organic compounds or favor microbial growth, enhancing N retention. Consequently, upper intertidal zones tend to accumulate higher OM stocks due to increased autochthonous and allochthonous inputs and comparatively lower degradation rates.

4.2 Sediment inorganic nutrient pools

In coastal sediments, inorganic nutrient concentrations reflect a dynamic balance between remineralization of organic matter, microbial uptake, adsorption to sediment particles, and exchanges with the overlying water column. These nutrients occur in several pools (PW, IC and EX), which are subject to distinct ecological and biogeochemical controls (García-Robledo et al., 2010, 2016; Stief et al., 2013). Most previous studies have focused on dissolved inorganic nutrients in the PW (Kristensen et al., 2008; Tay et al., 2013), while fewer have explored the role of IC and EX pools (García-Robledo et al., 2010, 2016; Stief et

al., 2013, 2022). In the Gulf of Nicoya intertidal sediments, the relative contributions of the different pools varied substantially (Table 2). The majority of PO_4^{3-}, NH_4^+, and DSi were found in the IC pool (88%, 75%, and 62% of their total sediment contents, respectively), indicating a strong association with microbial biomass. In contrast, NO_3^- was mainly present in the PW pool (67.6%), reflecting a higher potential for exchange with the water column. Nitrite (NO_2^-) showed the lowest total concentration (5.4 ± 3.1 nmol cm^{-2}) and was largely associated with the EX pool (83%), likely adsorbed to sediment particles. Given its role as a transient intermediate in nitrogen cycling, the low NO_2^- levels indicate tight coupling among nitrification and nitrate reduction processes.

In Punta Morales, concentrations of inorganic nutrients in the PW, IC, and EX pools was within the wide range reported from 14 other tidal flats in the inner Gulf of Nicoya (Corzo et al., 2024). Despite site-to-site variability related to geomorphological and hydrodynamic differences, the general distribution patterns among nutrient pools were consistent. Comparisons with temperate tidal flats are constrained by the limited data available, but studies in the Bay of Cádiz revealed higher seasonal maxima for NH_4^+, up to one order of magnitude greater than in the Gulf of Nicoya, as well as higher NO_3^- concentrations in both PW and EX pools (García-Robledo et al., 2010, 2016). However, PO_4^{3-} concentrations were similar between tropical and temperate flats in PW, though markedly higher in IC and EX pools in the temperate system. Sediment nutrients in the PW pool represent a potential source for the water column supporting pelagic primary production. In Punta Morales tidal flat, concentrations of NH_4^+, NO_3^- and PO_4^{3-} in the upper 0.5 cm of sediment PW were higher than in the overlying water column, while the contrary was observed for DSi (Soria-Píriz et al., 2017). This suggests a potential net efflux of nitrogen and phosphorus from the sediment

to the water column. However, this pattern may reverse in tidal flats located closer to the estuary's head, where nutrient concentrations in the water column are typically higher (Soria-Píriz et al., 2017, 2024).

SL can affect inorganic nutrient cycling and availability within the sediment, through its effect on the origin of sedimentary OM, the sediment grain size distribution and, therefore, the OM mineralization rates and pathways. Nutrient concentrations in the three pools did not change consistently with SL. NH_4^+, NO_3^-, and NO_2^- in their dominant pools (IC, PW, and EX, respectively) tended to increase with SL, as did DSi in the PW pool. Conversely, PO_4^{3-}-IC and DSi-EX decreased significantly with SL (Fig. 3, Fig. S1). The mechanisms driving these patterns remain uncertain due to the scarcity of comparable data, especially for IC and EX pools. In a North Sea sandy intertidal flat, concentrations of DSi, NH_4^+, and PO_4^{3-} in PW were an order of magnitude higher at lower SL than at higher SL (Billerbeck et al., 2006), suggesting that sediment type and local hydrodynamics modulate the magnitude and direction of nutrient fluxes. DistLM analysis for Punta Morales indicated that PW nutrient concentrations explained only a small portion of the variability in net primary production (NPP), respiration (RD), and chlorophyll *a* (Chla) (Tables S1–S2). Thus, MPB biomass and productivity in this system appear not to be limited by dissolved nutrients in the pore water.

4.3 Microphytobenthos abundance and community composition

Chlorophyll *a* content in Punta Morales tidal flat sediments (6.3 ± 3.9 μg Chla cm^{-2}) was among the highest recorded in the Gulf of Nicoya (Corzo et al., 2024) and within the range reported for other tropical and temperate tidal flats (MacIntyre et al., 1996; Benny et al 2021; García-Robledo et al., 2016; Kwon et al., 2020; Haro et al., 2020; Salleh & McMinn, 2021).

Chla increased with SL, in parallel with MPB abundance (Fig. 4), suggesting that MPB are the primary contributors to sedimentary Chla in this tropical intertidal system (Fig. S1). This is also supported by Chla:Pheo ratio, which increased landward, indicating a higher fraction of photosynthetically active Chla (Sun et al., 1993), and therefore more active MPB communities at high SL. Conversely, lower Chla:Pheo ratios seaward point to a larger proportion of degraded or detrital pigments, consistent with reduced MPB abundance and productivity in the lower intertidal (Fig. 4). The lower daily light availability at low SL and higher grazing pressure during longer immersion periods likely explain to the increase of MPB biomass with SL. DistLM analysis identified SL, mud content, and diatom percentage as the main drivers of Chla variability, while inorganic nutrients played a minor role (Tables S2–S3).

It must be borne in mind that DistLM analysis was done on a data set that it does not include seasonal variability or little, since both transects were done during the dry season, although in two consecutive years. Previous work using remote sensing has shown that MPB biomass and cover followed a clear seasonal pattern in the Guf of Nicoya despite interannual variability, with a seasonal peak in late wet and early dry seasons (November–December) and a clear decrease from December to April (Haro et al 2025). The analysis of the variability of MPB net primary production, respiration and Chla in 14 different tidal flats, sampled during dry and wet seasons, showed that in addition to SL, seasonal changes in rainfall and irradiance were their major seasonal drivers (Corzo et al. 2024). Higher nutrients availability during the rainy season and higher level of photo- and thermoinhibition during the emersion period in the dry season might explained the observed pattern (Savelli et al., 2021; Salleh and McMinn, 2021; Haro et al., 2020).

MPB abundance ranged from $1.9 \pm 0.4 \times 10^5$ cells cm^{-3} (Transect B) to $9.4 \pm 4.7 \times 10^5$ cells cm^{-3} (transect A) in the upper 0.5 cm of sediment (Table 1). These values are comparable to those found in temperate tidal flats and mangrove intertidal sediments (MacIntyre et al., 1996; García-Robledo et al., 2012; Benny et al., 2021). In addition to an increase of MPB abundance with SL (Fig. 4), MPB abundance was positively correlated with NH_4^+ and NO_3^- in the IC pool, and with NH_4^+ and DSi in the PW pool (Table S1). This is consistent with previous findings that MPB communities and associated microbes can store and utilize multiple forms of inorganic nutrients (García-Robledo et al., 2010, 2016; Stief et al., 2013; Kamp et al., 2015; Stief et al., 2022). The strong relationship between MPB abundance and DSi is expected, as diatoms require silica for frustule formation and primary production (Leynaert et al., 2011; Bohórquez et al., 2019). However, no statistically clear correlations were found between MPB abundance and any PO_4^{3-} pool, contrary to results from the Gulf of Nicoya and Bay of Cádiz, where Chla was correlated with several phosphate pools (García-Robledo et al., 2016; Corzo et al., 2024). This suggests that, at the time of sampling, MPB growth in Punta Morales was not limited by phosphate availability.

The MPB community in the Punta Morales tidal flat was dominated by pennate diatoms (47–81%) and cyanobacteria (12–52%). Diatoms were relatively more abundant in transect B and at low SL, whereas the proportion of cyanobacteria increased landward, leading to a transition from diatom dominance in the lower intertidal to co-dominance with cyanobacteria towards the upper intertidal (Fig. 4). This spatial shift in MPB community composition with respect to SL has been observed in temperate tidal flats as well. Cyanobacteria generally exhibit greater tolerance to desiccation, temperature fluctuations, and salinity stress, as well as higher metabolic flexibility (Wieland & Kühl, 2000; García de Lomas et al., 2005). Such

traits confer competitive advantage to cyanobacteria in the upper intertidal, where abiotic variability and exposure stress are greatest. In contrast, diatoms are favored at low SL, due to more stable environmental conditions, including a shorter emersion period, and their higher resistance to grazing (Fenchel, 1998). Overall, MPB abundance and community composition, i.e. the contribution of cyanobacteria and diatoms, with respect to SL, does not differ between temperate and tropical tidal flats.

4.4. Sediment net metabolism

Sediment net metabolism in the Punta Morales tidal flat was quantified from oxygen microprofiles under light and dark conditions (Fig. 5). Oxygen consumption in sediments integrates both aerobic mineralization of organic matter and the oxidation of reduced compounds (Fe^{2+}, H_2S, NH_4^+, CH_4 etc.) produced by anaerobic processes in the underlying anoxic zone (Glud 2008). The contrasting O_2 profiles in light and dark clearly illustrate the key role of MPB photosynthetic activity in controlling oxygen dynamics, markedly increasing O_2 availability and deepening the oxic layer within the sediment. The depth of the oxic zone (z_{ox}) increased by 1–2 mm in light, particularly in the middle and lower intertidal of transect B, where sediments contained a lower proportion of fine particles (Fig. 2, 5). This deeper oxygen penetration likely results from greater light availability in these coarser sediments, which allows photosynthesis to occur at deeper layers (MacIntyre et al., 1996; Cartaxana et al., 2016; Haro et al., 2019, 2024). In the absence of bioturbation, z_{ox}, which depends on oxygen supply, organic matter content, and sediment porosity, is a critical determinant of sediment biogeochemistry because it regulates organic matter mineralization pathways and rates (Glud, 2008). The shape and magnitude of O_2 profiles at Punta Morales resemble those observed in temperate tidal flats with similar grain sizes and organic matter

levels (Cartaxana et al 2016; Corzo et al., 2009; García-Robledo et al., 2010; Walpersdorf et al., 2017).

Net primary production and dark respiration rates ranged from 0.5–5.8 mmol O_2 m^{-2} h^{-1} and 0.6–2.7 mmol O_2 m^{-2} h^{-1}, respectively. These values are comparable to those reported for other tidal flats in the Gulf of Nicoya (Corzo et al., 2024), as well as for tropical and temperate intertidal zones worldwide (Kristensen et al., 2000; Oliveira et al., 2011; Underwood & Kromkamp, 1999; Kwon et al., 2014; Haro et al., 2020; Pérez-Rodríguez, 2024). Both NPP and RD increased with SL, although NPP exhibited a steeper slope being the upper intertidal more net autotrophic. NPP and RD were positively correlated with MPB abundance (total, diatom, and cyanobacterial fractions; Fig. 6c–d), as well as with the Chla:Pheo ratio, but not with total Chla (Fig. S1). The lack of correlation with Chla suggests that part of the measured Chla might not be fully active. The positive relationship between NPP and Chla:Pheo supports the use of this ratio as an indicator of physiologically active chlorophyll. The clear positive dependence of NPP and RD on SL was observed including different flats sampled during the wet and dry season. That survey showed that a substantial fraction of NPP and RD variability depended on irradiance (negatively) and rainfall (positively), suggesting a clear seasonal dependence in addition to the spatial dependence respect to MSL (Corzo et al 2024). Overall, these results suggest that relationships between MPB biomass and metabolic rates with SL seems to change with season. While further *in situ* experimental work is needed to settle this question, the analysis by remote sensing of MPB NDVI and cover variability across SL during several years clearly showed the existence of seasonal changes in addition to interannual variability (Haro et al 2025). In Punta Morales tidal flats, Multivariate DistLM analysis indicated that NPP variability was mainly explained by SL and the percentage of

592 diatoms, followed by PW NH_4^+ and PO_4^{3-} concentrations as secondary predictors. In contrast,
593 RD variability was best explained by SL, mud content, and Chla, with distance to shoreline,
594 organic carbon, and NO_3^- explaining a lower percentage of variability (Tables S1–S2). In
595 Punta Morales, RD did not correlate significantly with total organic matter or OC but did
596 correlate with TN and NH_4^+-IN, suggesting that respiration is more closely linked to substrate
597 lability and N-rich organic matter than to total organic carbon, which might include more
598 refractory fractions (Middelburg et al 1995).

599 In addition to its assessment by O_2 microprofiles, organic matter mineralization was directly
600 measured as TCO_2 accumulation in long-term incubations of sediment samples from transect
601 B. Volumetric mineralization rates did not vary significantly with depth (Fig. 7a), differing
602 from the typical decline with depth observed in many studies (Kristensen et al., 2000). Areal
603 mineralization rates, however, varied along the SL gradient, with higher values in the upper
604 intertidal (~1.3 mmol TCO_2 m^{-2} h^{-1}) and lower ones in the middle and lower zones (~0.5
605 mmol TCO_2 m^{-2} h^{-1}) (Fig. 7b). This pattern may reflect the higher lability of organic matter
606 in the upper intertidal, where MPB-derived production with lower C:N ratio represents a
607 greater fraction of total organic matter. The range of mineralization rates observed at Punta
608 Morales tidal flat was slightly lower than those reported for subtidal sediments along the Gulf
609 of Nicoya estuarine gradient (1.2–5.5 mmol TCO_2 m^{-2} h^{-1}; Gómez-Ramírez et al., 2019).
610 However, Gómez-Ramírez et al. (2019) used short-term whole core incubations that likely
611 resulted in higher rates due to the absence of limiting factors. Nonetheless, mineralization
612 rates in Punta Morales tidal flats are comparable to those measured in tropical intertidal
613 sediments of Phuket Island, Thailand (Kristensen et al., 2000), but notably lower than in
614 temperate intertidal flats such as the Westerschelde Estuary, Netherlands (Middelburg et al.,

615 1996). In addition, despite the long TCO_2 incubation time with respect to the quicker
616 measurements of O_2 consumption with microsensors in dark conditions, the mineralization
617 rates were comparable, assuming a mineralization stoichiometry in aerobic conditions of
618 $106C:138O_2$, similar to that of phytoplankton.

619

620 **5. Conclusions**

621 This study highlights the pivotal role of SL in shaping the ecological and biogeochemical
622 characteristics of tropical intertidal sediments in the Punta Morales mudflats in inner basin
623 of the Gulf of Nicoya. Along the intertidal gradient, sediment granulometry, organic matter
624 content, inorganic nutrient pools, and MPB abundance, community composition, biomass
625 and net metabolism all exhibited systematic changes linked to elevation. Sediments at higher
626 SL positions were characterized by finer grain sizes, while coarser particles dominated the
627 lower intertidal, reflecting selective sedimentation and resuspension processes driven by
628 variations in hydrodynamic energy. The contents of OM, OC, and TN increased with SL,
629 likely due to a combination of factors: greater inputs of allochthonous organic matter from
630 adjacent mangroves, enhanced autochthonous MPB production, and higher capacity of fine-
631 grained sediments to preserve organic matter. MPB abundance, % cyanobacteria, NPP and
632 RD rates increased with SL. NPP and RD rates were comparable to those reported for other
633 tropical and temperate tidal flats. Overall, this study demonstrates that both biological and
634 biogeochemical properties of tropical intertidal sediments vary markedly over short spatial
635 scales as a function of elevation within the tidal range. These fine-scale gradients result from
636 the complex and season dependent interplay between hydrodynamics, sediment texture,

637 nutrient availability, and MPB community structure and abundance. Considering this
638 zonation and its seasonal variability, it is essential for accurately scaling up site-specific
639 measurements to system level and for improving estimates of the contribution of intertidal
640 sediments to the overall carbon and nutrient dynamics of coastal ecosystems.

641

642 **Acknowledgements**

643 This study was funded by the projects C / 023621/09, D / 031020/10, and A1 / 037457/11 of
644 the Spanish Agency for International Cooperation and Development (AECID), the projects
645 CTM2013-43857-R and P11-RNM- 7199 of the Spanish Ministry of Economy and
646 Competitiveness and the Junta de Andalucía and supported by project 808-B3-127 of the
647 University of Costa Rica (UCR). Eddy Gómez-Ramírez was financed by a grant from the
648 University of Costa Rica and by the MICITT-CONICIT of the Government of Costa Rica.
649 Julio Bohórquez was funded by an FPI grant (BES-2010-035711) from the Spanish Ministry
650 of Economy and Competitiveness. We thank all the colleagues and support team of the UCA
651 and CIMAR-UCR that contributed to the completion of this study for their personal and
652 logistical support. Authors thank Guillermo Papaspyrou for his contribution to the graphical
653 abstract.

654 **Authorship contribution statement (CRediT)**

655 A. Corzo: Conceptualization. validation, supervision, formal analysis, writing, review &
656 editing, funding acquisition.

657 E. Gómez-Ramírez: Sampling, biogeochemical analysis, writing – original draft,
658 visualization, methodology, writing, review & editing.

659 E. García-Robledo: Validation, supervision, formal analysis, writing – review & editing.

S. Haro: Methodology, formal analysis, visualization, writing – original draft, writing, review & editing.

J. Bohórquez-Ferrando. Sampling, biogeochemical analysis, methodology, writing – original draft. review & editing.

J. L. Jiménez-Arias. Sampling, biogeochemical analysis, methodology, review & editing.

S. Papaspyrou: Validation, resources, data curation, statistics analysis, conceptualization, writing – review & editing.

Declaration of competing interest

The authors declare that they have no known competing financial interests or personal relationships that could have appeared to influence the work reported in this paper.

Data availability

Data will be made available on request without undue reservation.

References

Benny et al. 2021. Community Structure of Microphytobenthos Associated with Mangrove Ecosystems Along the Southwest Coast of India. Estuaries and Coasts (2021) 44:1380–1391.

Billerbeck et al 2006 Nutrient release from an exposed intertidal sand flat. Mar Ecol Prog Ser 316: 35–51, 2006

Bishop-Taylor R., Sagar S., Lymburner L., Beaman R.J. (2019). Between the tides: modelling the elevation of Australia's exposed intertidal zone at continental scale. *Estuarine, Coastal and Shelf Science*, 223, 115–128. doi:10.1016/j.ecss.2019.03.006.

684 Bohórquez J, McGenity TJ, Papaspyrou S, García-Robledo E, Corzo A and Underwood GJC
685 (2017) Different Types of Diatom-Derived Extracellular Polymeric Substances Drive
686 Changes in Heterotrophic Bacterial Communities from Intertidal Sediments. Front.
687 Microbiol. 8:245. doi: 10.3389/fmicb.2017.00245
688 Bohorquez, J., Calenti, D., García-Robledo, E., Papaspyrou, S., Jimenez-Arias, J.L.,
689 Gomez-Ramírez, E.H., Corzo, A., 2019. Water column dissolved silica concentration
690 limits microphytobenthic primary production in intertidal sediments. J. Phycol. 55,
691 625–636
692 Brito, A.C., Benyoucef, I., Jesus, B., Brotas, V., Gernez, P., Mendes, C.R., Launeau, P.,
693 Dias, M.P., Barillé, L., 2013. Seasonality of microphytobenthos revealed by
694 remotesensing in a South European estuary. Continent. Shelf Res. 66, 83–91.
695 Cartaxana, P. et al., 2016. Regulation of Intertidal Microphytobenthos Photosynthesis Over
696 a Diel Emersion Period Is Strongly Affected by Diatom Migration Patterns. *Front.*
697 *Microbiol.7:872. doi: 10.3389/fmicb.2016.00872*
698 Cheng Y., Andersen O.B. (2011). Multimission empirical ocean tide modeling for shallow
699 waters and polar seas. *Journal of Geophysical Research*, 116:C11.
700 doi:10.1029/2011JC007172.
701 Cloern, J.E., Foster, S.Q. & Kleckner, a. E., 2014. Phytoplankton primary production in the
702 world's estuarine-coastal ecosystems. *Biogeosciences*, 11(9), pp.2477–2501.
703 Corzo, A., van Bergeijk, S. A., García-Robledo, E. (2009). Effects of green macroalgal
704 blooms on intertidal sediments: Net metabolism and carbon and nitrogen contents. Mar
705 Ecol. Prog. Ser. 380: 81-93.
706 Corzo, A., Haro, S., Gómez-Ramírez, E., González, C.J., Papaspyrou, S., Garcia-Robledo,
707 E., 2024. Intertidal microphytobenthic primary production and net metabolism of a

tropical estuary. Mar. Environ. Res. 202, 106741. https://doi.org/

Daggers, T.D., Herman, P.M.J., Van Der Wal, D., 2020. Seasonal and spatial variability in patchiness of microphytobenthos on intertidal flats from sentinel-2 satellite imagery. Front. Mar. Sci. 7, 1–14.

de Jonge, V. N. 1980. Fluctuations in the organic carbon to chlorophyll a ratios for estuarine benthic diatom populations Mar. Ecol. prog. Ser. 2: 345-353.

Fenchel T (1998) Formation of laminated cyanobacterial mats in the absence of benthic fauna. Aquat Microb Ecol 14: 235–240

Friedrichs, C.T., 2011. Tidal Flat Morphodynamics: A Synthesis. In: Eric Wolanski, E., McLusky, D. (Eds.), Treatise on Estuarine and Coastal Science. Academic Press, pp. 137–170. https://doi.org/10.1016/B978-0-12-374711-2.00307-7.

García de Lomas, J., Corzo, A., García, C.M., van Bergeijk S.A. (2005). Microbenthos in a hypersaline tidal lagoon: factors affecting microhabitat, community structure and mass exchange at the sediment-water interface. Aquat. Microb. Ecol. 38: 53-69.

García-Robledo et al 2012. Photosynthetic activity and community shifts of microphytobenthos covered by green macroalgae. Environmental Microbiology Reports (2012) 4(3), 316–325

García-Robledo E, Bohórquez J, Corzo A, Jiménez-Arias JL, Papaspyrou S, 2016. Dynamics of Inorganic Nutrients in Intertidal Sediments: Porewater, Exchangeable, and Intracellular Pools. Front. Microbiol. 7:761.

García-Robledo, E. et al., 2010. Freeze-lysable inorganic nutrients in intertidal sediments: Dependence on microphytobenthos abundance. *Marine Ecology Progress Series*, 403, pp.155–163.

García-Robledo, E., Corzo, A. & Papaspyrou, S., 2014. A fast and direct spectrophotometric

732 method for the sequential determination of nitrate and nitrite at low concentrations in
733 small volumes. *Marine Chemistry*, 162(3), pp.30–36.
734 Glud, R.N. 2008. Oxygen dynamics of marine sediments. Mar Biol. Res 4:243-289
735 Gomez-Ramirez, E.H., Corzo, A., Garcia-Robledo, E., Bohorquez, J., AgüeraJaquemet, A.,
736 Bibbo-Sanchez, F., Soria-Piriz, S., Jimenez-Arias, J.L., Morales, A.,
737 Papaspyrou, S., 2019. Benthic-pelagic coupling of carbon and nitrogen along a
738 tropical estuarine gradient (Gulf of Nicoya, Costa Rica). Estuar. Coast Shelf Sci. 228,
739 106362.
740 Grasshoff, K., Ehrhardt, M. & Kremling, K., 1993. Methods of Seawater Analysis. Hall,
741 P.O.J. & Aller, R.C., 1992. Rapid, small volume, flow injection analysis for CO2 and
742 NH4+ in marine and freshwaters. *Limnol. Oceanogr.*, 37(5), pp.1113–1119.
743 Haro S, Lara M, Laiz I, González CJ, Bohórquez J, Garcia-Robledo E, Corzo A and
744 Papaspyrou S (2020) Microbenthic Net Metabolism Along Intertidal Gradients (Cadiz
745 Bay, SW Spain):Spatio-Temporal Patterns and Environmental Factors. Front. Mar. Sci.
746 7:39.
747 Haro et al 2022. Microphytobenthos spatio-temporal dynamics across an intertidal
748 gradient using Random Forest classification and Sentinel-2 imagery. Science of the
749 Total Environment 804 (2022) 149983
750 Haro et al 2025. Microphytobenthos spatio-temporal dynamics across an intertidal gradient
751 in a tropical estuary using Sentinel-2 imagery. Science of the Total Environment 963
752 (2025) 178516. https://doi.org/10.1016/j.scitotenv.2025.178516.
753 Hedges,J.I., Keil, R.G. 1995. Sedimentary organic matter preservation: an assessment and
754 speculative synthesis. Marine Chemistry 49 (1995) 81-115
755 Hedges, J.I., Keil, R.G., and Berner, R. 1997. What happens to terrestrial organic matter in

the ocean? Org. Goechem 27:195-212.

Heiri, O., Andre, L. & Lemcke, G., 2001. Loss on Ignition as a Method for Estimating Organic and Carbonate Content in Sediments : Reproducibility and Comparability of Results. , (DECEMBER), pp.101–110.

Hillebrand, H. and Sommer, U. 1999. The nutrient stoichiometry of benthic microalgal growth: Redfield proportions are optimal. *Limnol. Oceanogr.,* 44(2), 1999, 440–446.

Hofmann, T., Hanlon, A. R. M., Taylor, J. D., Ball, A. S., Osborn, A. M. and Underwood G. J. C. (2009). Dynamics and compositional changes in extracellular carbohydrates in estuarine sediments during degradation. *Mar Ecol Prog Ser* 379, 45–58.

Hope et al 2020. The role of microphytobenthos in soft-sediment ecological networks and their contribution to the delivery of multiple ecosystem services. Journal of Ecology. 2020;108:815–830.

Kamp, A., Høgslund, S., Risgaard-Petersen, N., and Stief, P. (2015). Nitrate storage and dissimilatory nitrate reduction by eukaryotic microbes. *Front. Microbiol.* 6:1492. doi: 10.3389/fmicb.2015.01492

Keil, R.G., Tsamakis, E., Wolf, N., Hedges, J.I., Goñi, M., 1997. Relationships between organic

carbon preservation and mineral surface area in Amazon fan sediments (holes 932A and 942A). In: Flood, R.D., Piper, D.J.W., Klaus, A., Peterson, L.C. (Eds.), Proc. ODP, Scientific Results, vol. 155, pp. 531–538

Kristensen, E. et al., 2000. Carbon and nitrogen mineralization in sediments of the Bangrong mangrove area, Phuket, Thailand. *Aquatic Microbial Ecology*, 22(2), pp.199–213.

Kristensen, E. et al., 2008. Organic carbon dynamics in mangrove ecosystems: A review. *Aquatic Botany*, 89(2), pp.201–219.

780 Kühl, M., Glud, R.N., Ploug, H., Ramsing, N.B., 1996. Microenvironmental control of
781 photosynthesis and photosynthesis-coupled respiration in an epilithic cyanobacterial
782 biofilm. J. Phycol. 32, 799–812.
783 Kwon, B.-O. et al., 2014. The Relationship between Primary Production of
784 Microphytobenthos and Tidal Cycle on the Hwaseong Mudflat, West Coast of Korea.
785 *Journal of Coastal Research*, 298, pp.1188–1196.
786 Kwon, B.-O., Kim, H., Noh, J., Yip, S., Nam, J., Seong, J., 2020. Spatiotemporal
787 variability in microphytobenthic primary production across bare intertidal flat ,
788 saltmarsh, and mangrove forest of Asia and Australia. Mar. Pollut. Bull. 151,
789 110707-110707.
790 Leynaert, A., Longphuirt, S.N., An, S., Lim, J.-H., Claquin, P., Grail, J., Kwon, B.O.,
791 Koh, C.H., 2011. Tidal variability in benthic silicic acid fluxes and
792 microphytobenthos uptake in intertidal sediment. Estuar. Coast Shelf Sci. 95, 59–66.
793 Lin, W.-J., Wu, J., Lin, H.-J., 2020. Contribution of unvegetated tidal flats to coastal
794 carbon flux. Global Change Biol. 26, 3443–3454.
795 MacIntyre, H.L., Geider, R.J., Miller, D.C., 1996. Microphytobenthos: the ecological role
796 of the “Secret Garden” of unvegetated, shallow-water marine habitats. I.
797 Distribution, abundance and primary production. Estuaries 19, 186. https://doi.org/
798 10.2307/1352224.
799 Mayer, L.M., 1999. Extent of coverage of mineral surfaces by organic matter in marine
800 sediments. Geochimica et Cosmochimica Acta, Vol. 63, No. 2, pp. 207–215, 1999.
801 McFeeters S.K. (1996). The use of the normalized difference water index (NDWI) in the
802 delineation of open water features. *International Journal of Remote Sensing*, 17(7),
803 1425–1432. doi:10.1080/01431169608948714.

804 Middelburg, J.J. et al., 1995. Carbon and nitrogen cycling in intertidal sediments near Doel,
805 Scheldt Estuary. *Hydrobiologia*, 311(1–3), pp.57–69.
806 Middelburg, J. J., Klaver, G., Nieuwenhuize, J., Wielemaker, A., de Haas, W., Vlug, T., van
807 der Nat, J.F.W.A. 1996. Organic matter mineralization in intertidal sedimnets along an
808 estuarine gradient. Mar Ecol Prog Ser. 132:157-168.
809 Middelburg, J. J., Barranguet, C., Boschker, H. T. S., Herman, P. M. J., Moens, T., and Heip,
810 C. H. R. (2000). The fate of intertidal icrophytobenthos carbon: an in situ 13C-labeling
811 study. Limnol. Oceanogr. 45, 1224–1234. doi: 10.4319/lo.2000.45.6.1224
812 Murray, N.J., Phinn, S.R., Dewitt, M., Ferrari, R., Johnston, R., Lyons, M.B., Clinton, N.,
813 Thau, D., Fuller, R.A., 2019. The global distribution and trajectory of tidal flats.
814 Nature 565, 222–225.
815 Oliveira, V.P., Bento, L.F.J. & Prast, A.E., 2011. Short-term spatial and temporal variation
816 of sediment oxygen dynamics in a tropical tidal salt flat. *Wetlands Ecology and*
817 *Management*, 19(5), pp.389–395.
818 Orvain F, Lefebvre S, Montepini J, Sébire M, Gangnery A, Sylvand B, 2012. Spatial and
819 temporal interaction between sediment and microphytobenthos in a temperate estuarine
820 macro-intertidal bay. Mar. Ecol. Prog. Ser. 458:53–68.
821 Oviatt, C. a et al., 1986. A comparision of system (O2 and CO2) and C-14 measurements of
822 metabolism in estuarine mesocosms. *Marine Ecology Progress Series*, 28, pp.57–67.
823 Palter, J., Coto, S.L., Ballestero, D., 2007. The distribution of nutrients, dissolved oxygen
824 and chlorophyll a in the upper Gulf of Nicoya, Costa Rica, a tropical estuary. Rev.
825 Biol. Trop. 55, 427–436.
826 Pérez-Rodríguez V, Corzo A, Papaspyrou S, van Bergeijk SA, Vilas C, Cañavate JP and
827 Garcia-Robledo E (2024) Benthic metabolism and nutrient dynamics of a hyperturbid

828 and hypernutrified estuary. Front. Mar. Sci. 11:1389673. doi:
829 10.3389/fmars.2024.1389673
830 Ritchie, R.J., 2008. Universal chlorophyll equations for estimating chlorophylls a, b, c, and
831 d and total chlorophylls in natural assemblages of photosynthetic organisms using
832 acetone, methanol, or ethanol solvents. *Photosynthetica*, 46(1), pp.115–126.
833 Salleh, S and McMinn, A. 2021. Tolerance of tropical marine microphytobenthos exposed to
834 elevated irradiance and temperature. Biogeosciences, 18, 5313–5326, 2021
835 Sanders, C.J., Smoak, J.M., Naidu, A.S., Sanders, L.M., Patchineelam, S.R., 2010. Organic
836 carbon burial in a mangrove forest, margin and intertidal mud flat. Estuar. Coast
837 Shelf Sci. 90, 168–172.
838 Savelli, R., Serodio, ˆ J., Cugier, P., M´ el´eder, V., Polsenaere, P., Dupuy, C., Le Fouest, V.,
839 2021. Potential impact of photoinhibition on microphytobenthic primary production
840 on a large intertidal mudflat. J. Geophys. Res.: Biogeosciences 126, e2021JG006443
841 Seguro, I. et al., 2015. Seasonal changes of the microplankton community along a tropical
842 estuary. *Regional Studies in Marine Science*, 2(November), pp.189–202.
843 Soria-Píriz, S., García-Robledo, E., Papaspyrou, S., Aguilar, V., Seguro, I., Acuña, J.,
844 Morales, A., Corzo, A., 2017. Size fractionated phytoplankton biomass and net
845 metabolism along a tropical estuarine gradient. Limnol. Oceanogr. 62, S309–S326.
846 https://doi.org/10.1002/lno.10562.
847 Soria-Piriz et al 2024. Coupling between microbial assemblages and environmental drivers
848 along a tropical estuarine gradient. Science of the Total Environment 955 (2024) 177122
849 Stal, L.J., van Gemerden, H. & Krumbein, W.E., 1984. The simultaneous assay of
850 chlorophyll and bacteriochlorophyll in natural microbial communities. *Journal of*
851 *Microbiological Methods*, 2(6), pp.295–306.

852 Stief, P., Kamp, A., and De Beer, D. (2013). Role of diatoms in the spatial-temporal
853 distribution of intracellular nitrate in intertidal sediment. *PLoS ONE* 8:e73257.
854 doi: 10.1371/journal.pone.0073257
855 Stief et al 2022. Intracellular nitrate storage by diatoms can be an important nitrogen pool in
856 freshwater and marine ecosystems. COMMUNICATIONS EARTH &
857 ENVIRONMENT | (2022) 3:154 | https://doi.org/10.1038/s43247-022-00485-8
858 Tang, D., Liu, X., Xia, Z., Hou, J., Yang, X., Li, P., Yuan, X., 2023. Sources of organic
859 matter and carbon stocks in two mangrove sediment cores and surface sediment
860 samples from Qinglan Bay, China. Sci. Total Environ. 893, 164897
861 Tay et al 2013. Dissolved inorganic nitrogen concentrations in an estuarine tidal flat**.** Journal
862 of Coastal Research, Special Issue No. 65, 2013
863 Thompson, R.C. et al., 1999. Problems in extraction and spectrophotometric determination
864 of chlorophyll from epilithic microbial biofilms: towards a standard method. *Journal of*
865 *the Marine Biological Association of the United Kingdom*, 79, pp.551–558.
866 Ubertini, M., Lefebre, S., Rakotomalala, C., and Orvain, F. (2015). Impact of sediment grain-
867 size and biofilm age on Epipelic microphytobenthos resuspension. J. Exp. Mar. Biol.
868 Ecol. 467, 52–64. doi: 10.1016/j.jembe.2015.02.007
869 Underwood, G. J. C., and Kromkamp, J. (1999). Primary production by phytoplankton and
870 microphytobenthos in estuaries. Adv. Ecol. Res. 29, 93–153. doi: 10.1016/S0065-
871 2504(08)60192-0
872 Underwood, G. J. C., and Paterson, D. M. (2003). The importance of extracellular
873 carbohydrate production by marine epipelic diatoms. Adv. Bot. Res. 40,183–240. doi:
874 10.1016/S0065-2296(05)40005-1
875 Walpersdorf, E. et al., 2017. In situ oxygen dynamics and carbon turnover in an intertidal

876 sediment (Skallingen, Denmark). Marine Ecology Progress Series 566, pp.49–65.
877 Wieland A, Kühl M (2000) Short-term temperature effects on oxygen and sulfide cycling in
878 a hypersaline cyanobacterial mat (Solar Lake, Egypt). Mar Ecol Prog Ser 196:87–102.
879 Zou, H., Li, X., Li, S., Xu, Z., Yu, Z., Cai, H., Chen, W., Ni, X., Wu, E., Zeng, G., 2023. Soil
880 organic carbon stocks increased across the tide-induced salinity transect in restored
881 mangrove region. Sci. Rep. 13, 19758.
882
883

884 **Tables**

885

886 **Table 1.** Sea level range, intertidal slope and average (± standard deviation) of main
887 biogeochemical variables of surface intertidal sediment for transects A and B (n=3), and both
888 pooled together (Total, n=6). Intertidal slope for each transects is calculated as the slope of
889 the regression line between sea level and distance to shore expressed in %.

890

891

	Transect A	Transect B	Total
Sea level (m)	-0.65 to 0.00	-1.13 to -0.59	-1.13 to 0.00
Intertidal slope (%)	0.22	0.56	0.39 ± 0.24
% fine sediment	86.9 ± 11.8	81.2 ± 12.9	84.1 ± 12.4
OC (mg cm^{-2})	10.7 ± 0.86	8.4 ± 1.73	9.6 ± 1.75
TN (mg cm^{-2})	0.9 ± 0.08	0.7 ± 0.16	0.8 ± 0.16
OC:TN (mol:mol)	13.3 ± 1.76	13.0 ± 0.82	13.2 ± 1.35
Chla (μg cm^{-2})	8.1 ± 4.73	4.4 ± 1.50	6.3 ± 3.9
Chla:Pheo	0.6 ± 0.09	0.2 ± 0.05	0.4 ± 0.19
MPB (10^5 cells cm^{-3})	9.4 ± 4.7	1.9 ± 0.4	5.9 ± 4.9
% Diatoms	58.4 ± 11.99	70.5 ± 10.19	64.1 ± 12.39
P_N (mmol O_2 m^{-2} h^{-1})	2.7 ± 1.74	1.1 ± 0.54	2.0 ± 1.51
R_D (mmol O_2 m^{-2} h^{-1})	1.7 ± 0.58	1.3 ± 0.30	1.5 ± 0.50

892

893

894 **Table 2.** Concentrations of inorganic nutrients (nmol cm^{-2}) ± SD (n = 12-18) integrated in
895 the upper 0.5 cm sediment layer in pore water (PW) in the intracellular (IC) and in the
896 exchangeable (EX) pools. PO_4^{3-} was below detection limit (d. l.) in EX pool.

	NH_4^+	NO_2^-	NO_3^-	PO_4^{3-}	DSi
PW-pool	10.5 ± 16.6	0.8 ± 1.7	11.3 ± 13.4	4.5 ± 6.6	37.1 ± 9.6
IC-pool	150.8 ± 40.1	0.4 ± 0.4	4.6 ± 7.9	14.8 ± 5.6	106.3 ± 31.6
EX-pool	53.0 ± 12.0	4.5 ± 2.6	2.0 ± 3.5	< d. l.	36.8 ± 19.5
Total	200.7 ± 39.1	5.4 ± 3.1	16.7 ± 13.7	16.8 ± 6.4	170.2 ± 57.5

897
898
899
900
901
902
903
904
905
906
907
908

Figures

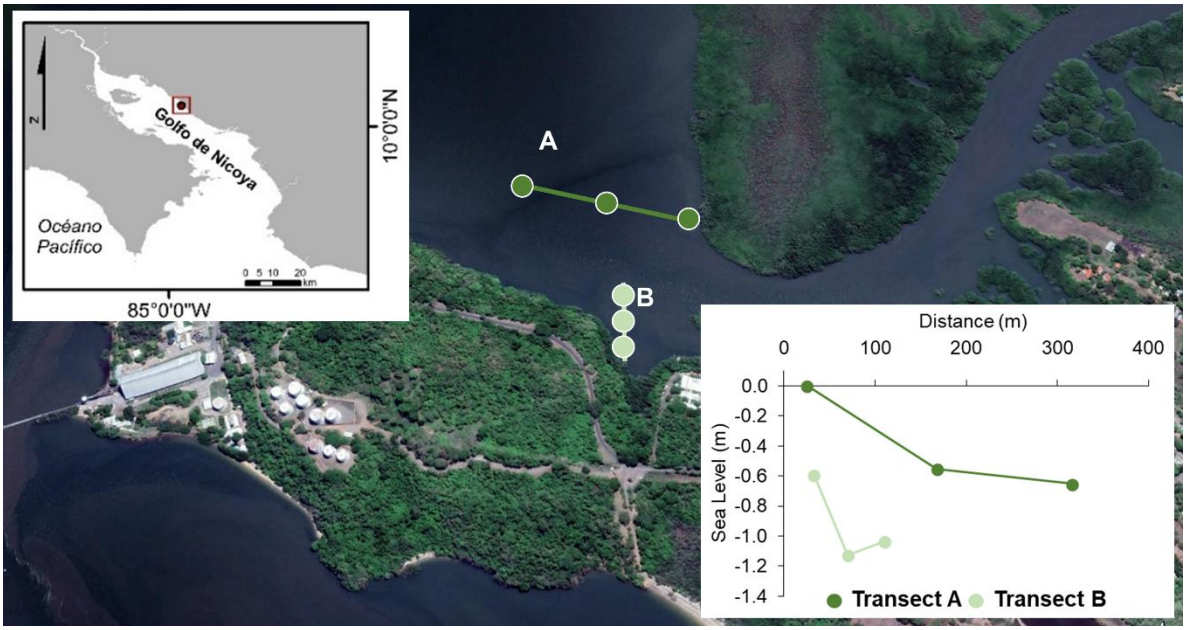


Fig 1. Location of transects A and B in the intertidal zones of Punta Morales, Gulf of Nicoya (Inserted map). Transects A and B presented different slopes as shown at sea level versus distance plots (inserted graph).

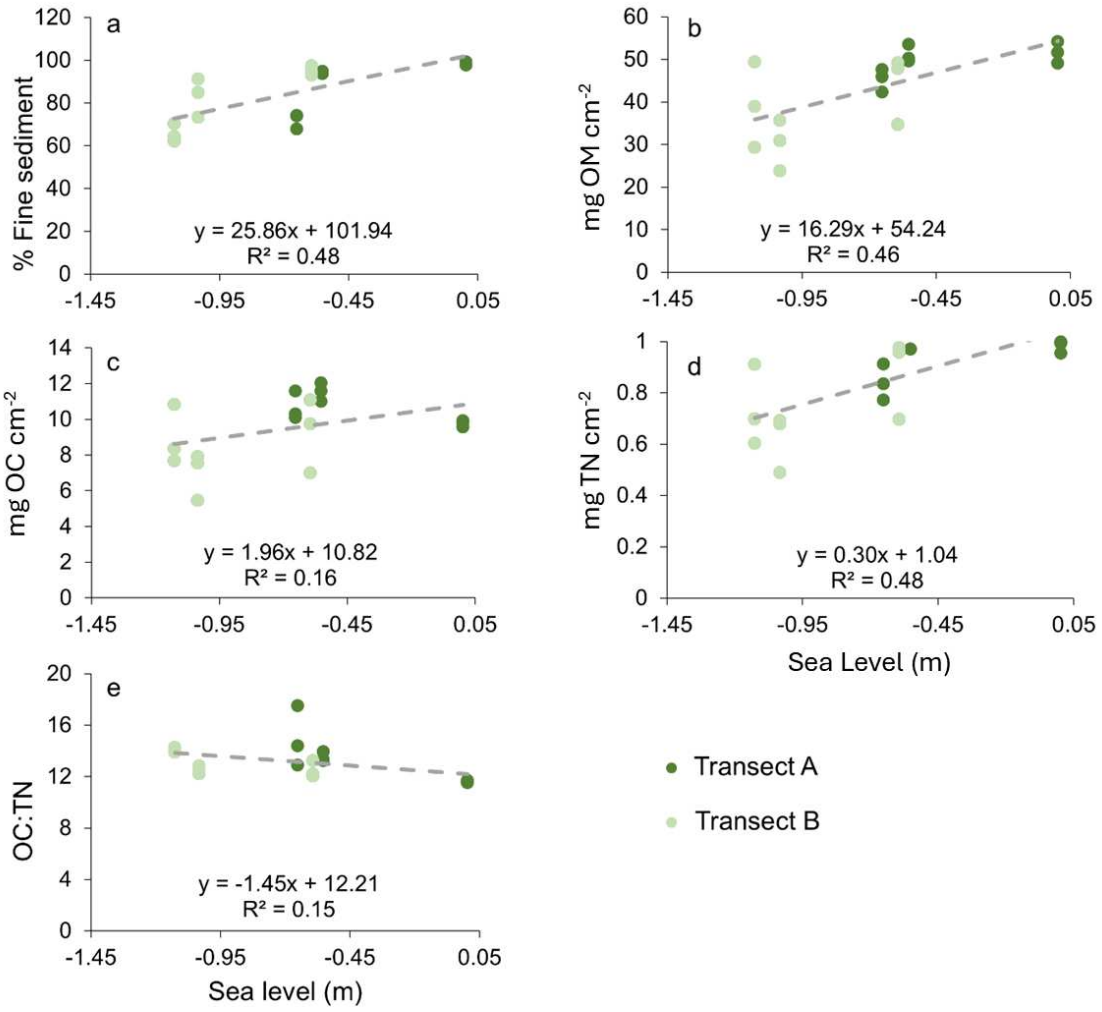
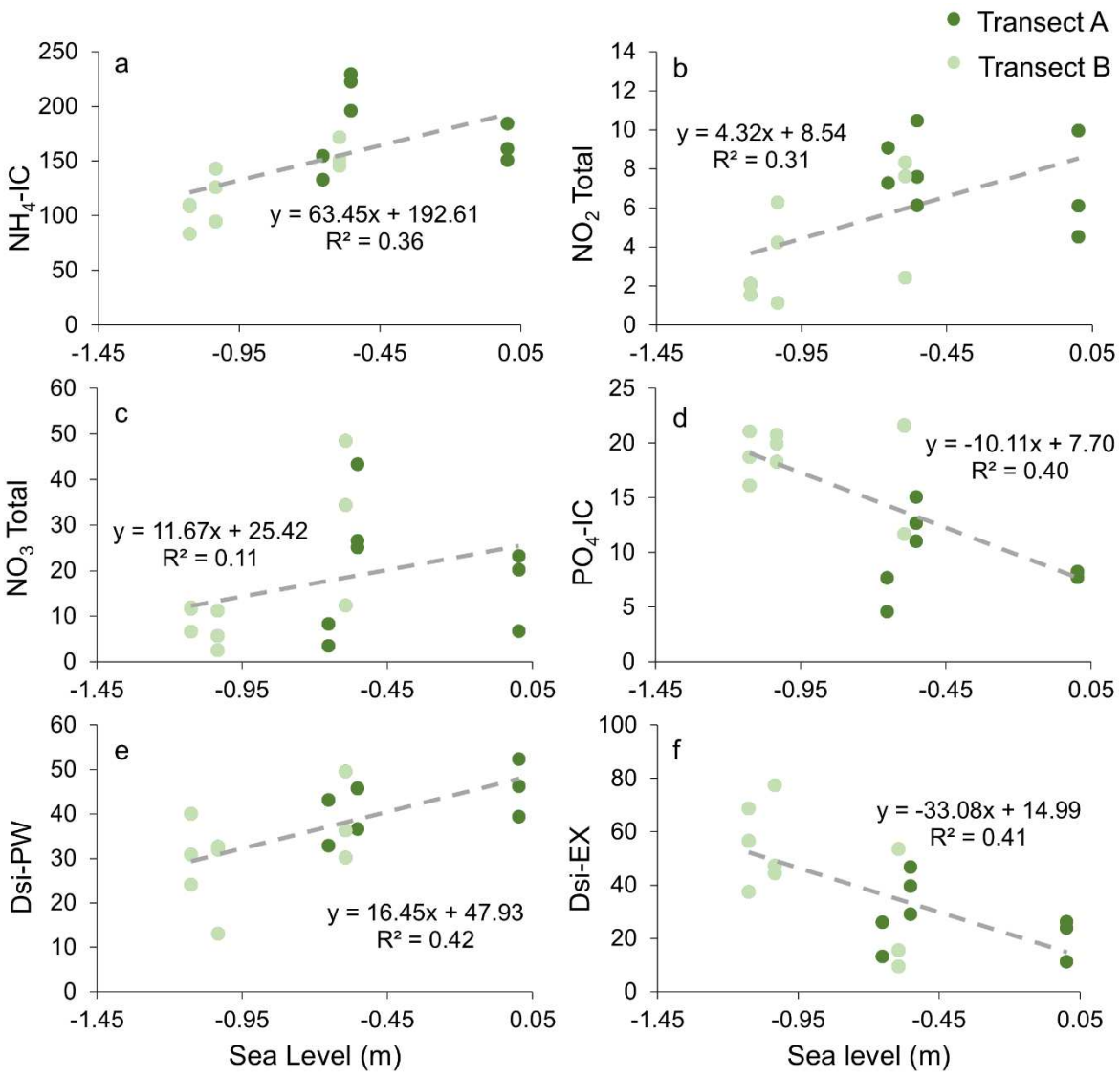


Fig 2. Percentage of fine sediment (<63 µm) (a), organic matter (mg OM cm^{-2}) (b), organic carbon (mg OC cm^{-2}), total nitrogen (mg TN cm^{-2}) and OC:TN ratio in transect A and B in the intertidal zone. Transect A and B are indicated in different colors. Regressions in plots a, b and d are statistically significant (n=18, $p<0.01$).

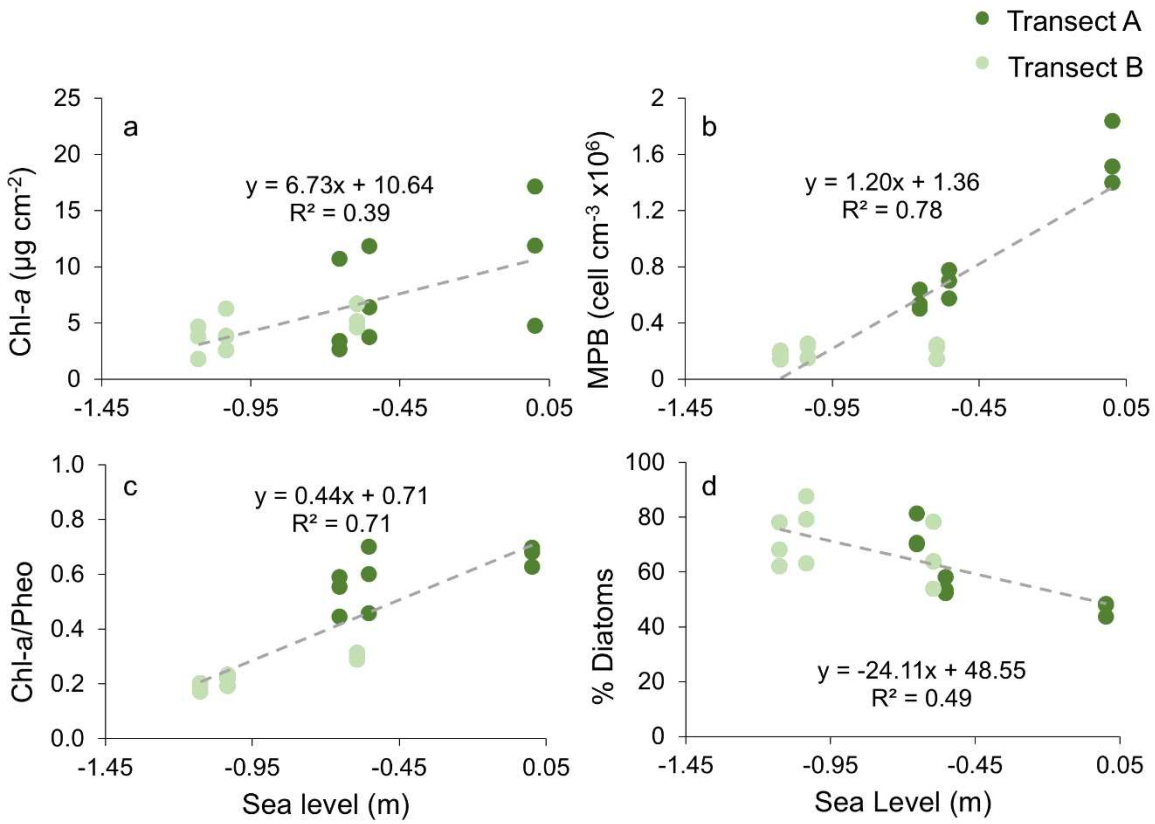


924

925 Fig. 3. Content of inorganic nutrients (nmol cm^{-2}) in different sediment pools respect to sea
926 level (SL, m) in both transects. NH_4^+ intracellular (a), NO_2^- total (b), NO_3^- total (c), PO_4^{3-}
927 intracellular (d), DSi in pore water (e) and DSi in the exchangeable pool (f). Transect A and
928 B are indicated in different colors.

929

930



931

932 Fig. 4. Changes in chlorophyll a (Chla, µg cm^{-2}), ratio Chlorophyll a: Pheophytin
933 (Chla:Pheo), abundance of microphytobenthos (MPB, cells cm-3) and percentage of diatoms
934 (%Diatoms) respect to sea Level (m) in the sediment of Punta Morales (Gulf of Nicoya).
935 Transect A and B are indicated in different colors.

936

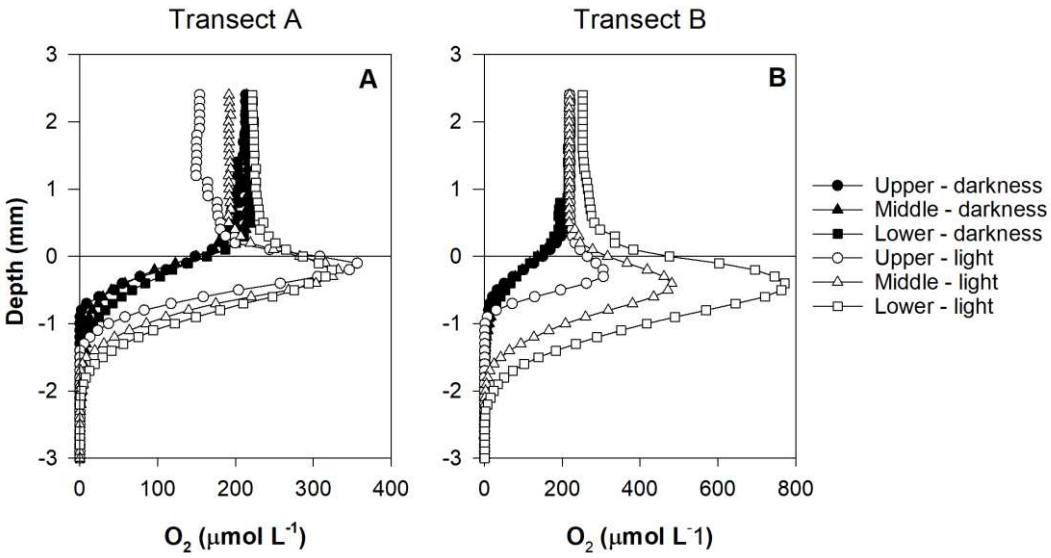
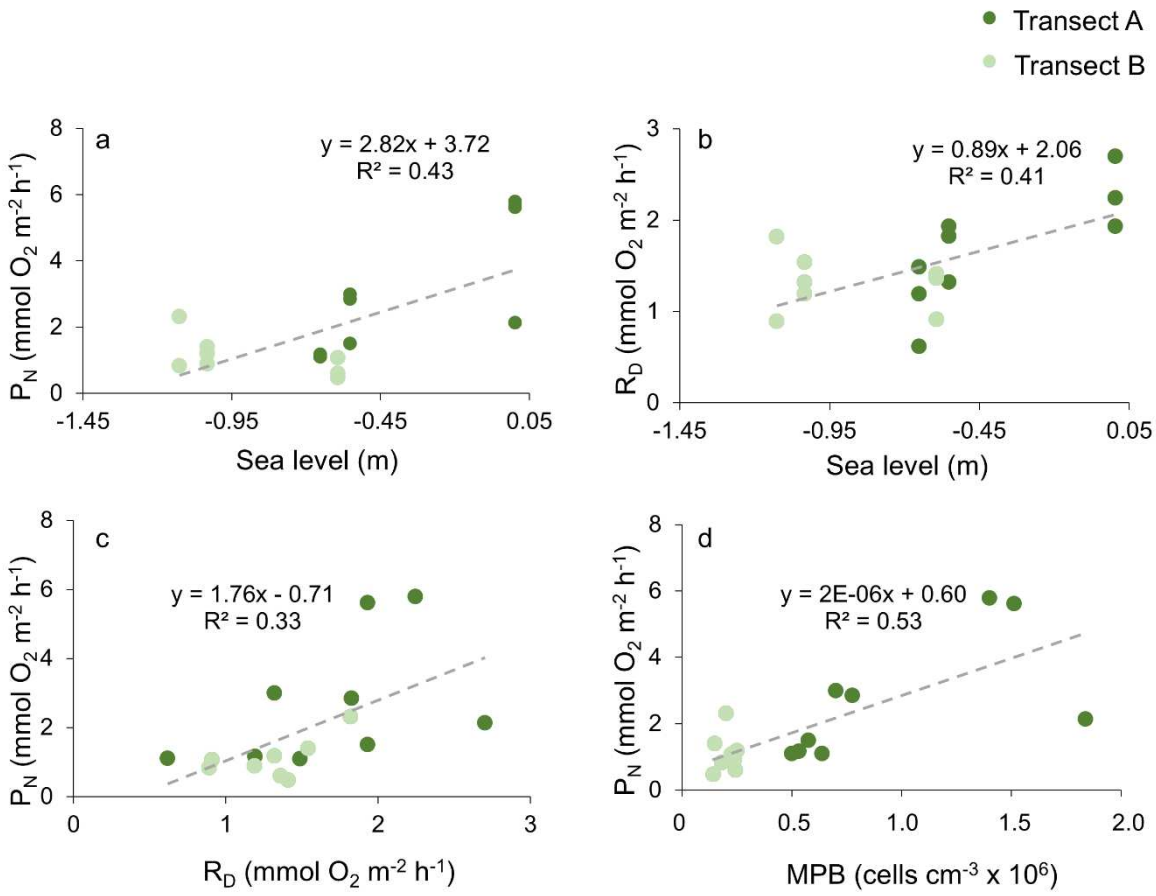


Figure 5. Mean oxygen profiles (n=3) in dark and light conditions. Points in the intertidal area are distinguished as upper, middle and low sea level. Error bars are not presented for the sake of clarity.



944

945 Figure 6. Sediment Net primary production in light (P_N, mmol O_2 m^{-2} h^{-1}) (a) and community
946 respiration in dark (RD, mmol O_2 m^{-2} h^{-1}) (b) respect to sea level (m). PN respect to RD (c)
947 and PN respect to MPB abundance (cells mL-1) (d). Transect A and B are indicated in
948 different colors.

949

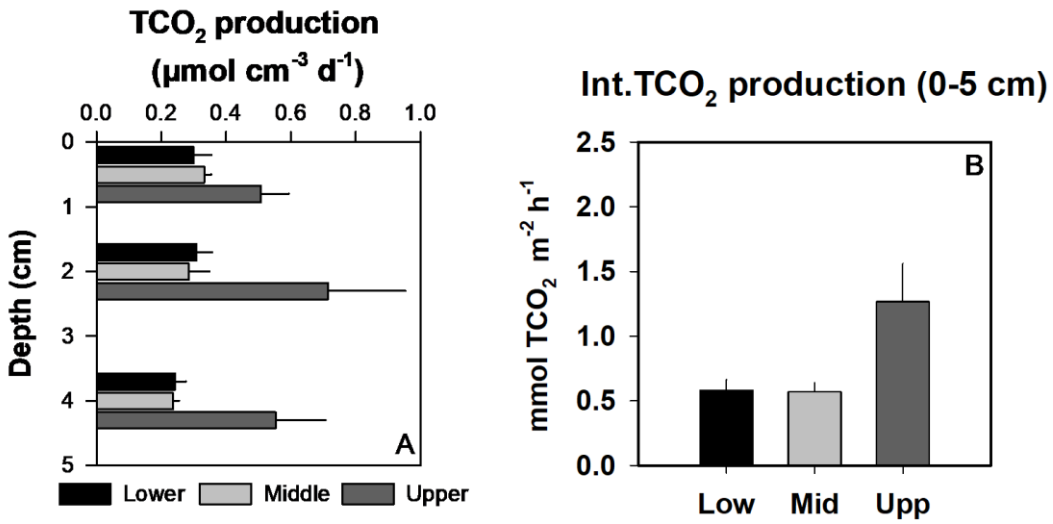


Fig. 7. Vertical CO_2 production (A) and integrated CO_2 production in the upper 5cm (B) during laboratory incubations of intertidal sediments of inner Gulf of Nicoya in transect B. CO_2 production was not measured in transect A.

960

961 **Supplementary material for:**

962 **Microphytobenthos primary production and organic matter mineralization along the**
963 **sea level gradient in a tropical mudflat**

964 Corzo[1,2]*, Alfonso, Eddy Gómez-Ramírez[1,3], Emilio Garcia-Robledo[1,2], Sara Haro[1,4], Julio
965 Bohórquez-Ferrando[1], Juan Luis Jiménez-Arias[1], Sokratis Papaspyrou[1,2].

966

967 [1] Departamento de Biología, Facultad de Ciencias del Mar y Ambientales, Universidad de
968 Cádiz, Pol. Río San Pedro s/n, 11510-Puerto Real, Cádiz, Spain.

969 [2] Instituto Universitario de Investigación Marina (INMAR), Campus Universitario de Puerto
970 Real, 11510, Cadiz, Spain

971 [3] Universidad de Costa Rica, Escuela de Química y CIMAR, San Pedro Montes de Oca,
972 11501-2060, San José, Costa Rica.

973 [4] Instituto Universitario de Investigación Marina (INMAR), Campus Universitario de
974 Puerto Real, 11510, Spain
975

976

977 * corresponding author: alfonso.corzo@uca.es

978

979

980

981

982

983

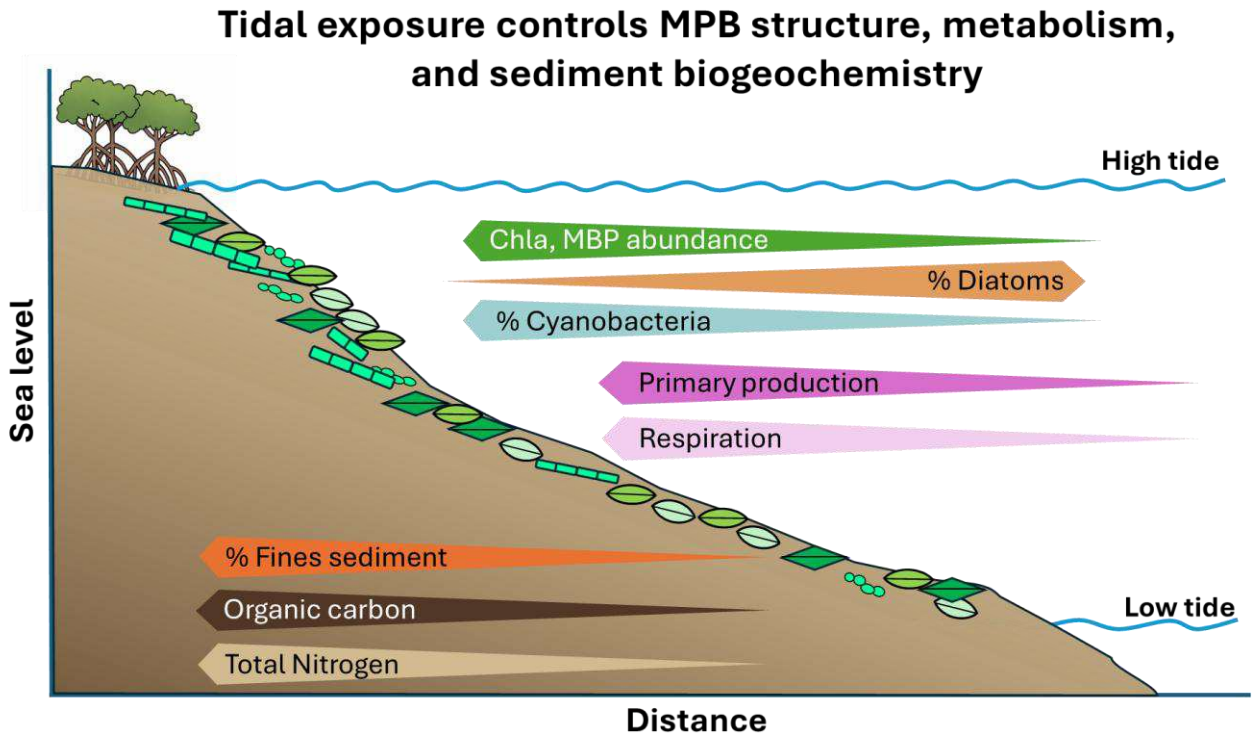
984

985

986

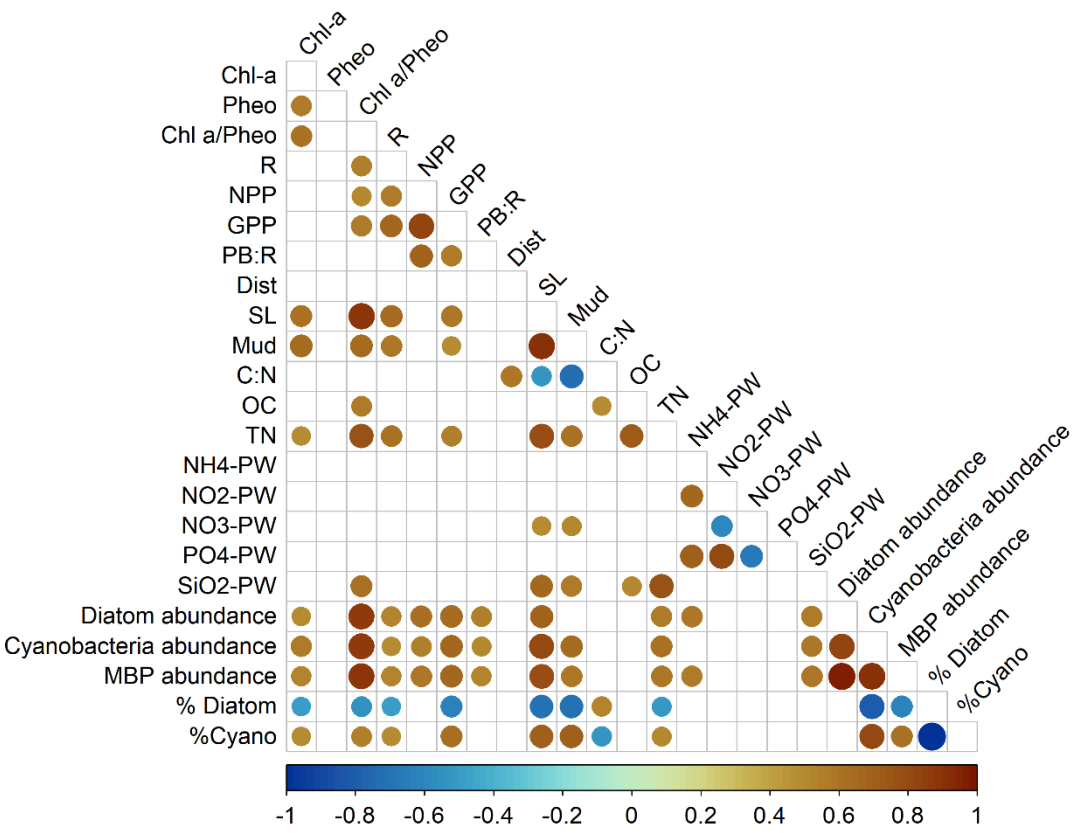
987 **Graphical abstract**

988



989

990



991

992

993 **Figure S1.** Correlation matrix between biological and physicochemical variables in the
994 surface layer of sediment across two intertidal transects at Punta Morales (Nicoya Gulf). The
995 color and size of each symbol indicate the Spearman correlation coefficient value, as shown
996 by the bottom color bar, with blue representing negative correlations and brown representing
997 positive correlations. Non-significant correlations are displayed as blank cells (i.e., p-value
998 > 0.05; n = 18).

999

1000

1001 **Table S1.** DistLM regression analysis marginal test results of benthic metabolism and microalgal
1002 biomass versus single explanatory variables.

	Variable	SS(trace)	Pseudo-F	P	Prop.
NPP	Dist	1.183	0.480	0.510	2.9%
	SL	**16.835**	**11.326**	**0.007**	**41.4%**
	<63um	6.236	2.902	0.102	15.4%
	C:N	4.765	2.126	0.184	11.7%
	OC	2.475	1.038	0.356	6.1%
	Chl-a	4.793	2.141	0.149	11.8%
	NH4-PW	0.025	0.010	0.936	0.1%
	NO3-PW	0.669	0.268	0.608	1.6%
	PO4-PW	0.020	0.008	0.931	0.1%
	SiO2-PW	3.544	1.530	0.220	8.7%
	% Diatom	**14.070**	**8.480**	**0.001**	**34.6%**
Rd	Dist	0.278	1.004	0.344	5.9%
	SL	**1.913**	**10.917**	**0.007**	**40.6%**
	Mud	**1.240**	**5.702**	**0.026**	**26.3%**
	C:N	0.825	3.389	0.075	17.5%
	OC	0.366	1.344	0.264	7.7%
	Chl-a	**1.307**	**6.134**	**0.019**	**27.7%**
	NH4-PW	0.211	0.750	0.420	4.5%
	NO3-PW	0.000	0.000	0.986	0.0%
	PO4-PW	0.361	1.325	0.269	7.6%
	SiO2-PW	0.718	2.873	0.114	15.2%

	% Diatom	**1.126**	**5.013**	**0.047**	**23.9%**
Chla	Dist	0.317	0.018	0.902	0.1%
	SL	**110.410**	**10.223**	**0.006**	**39.0%**
	Mud	**69.331**	**5.186**	**0.026**	**24.5%**
	C:N	5.656	0.326	0.573	2.0%
	OC	15.569	0.931	0.362	5.5%
	NH4-PW	58.469	4.162	0.061	20.6%
	NO3-PW	0.116	0.007	0.935	0.0%
	PO4-PW	49.641	3.400	0.089	17.5%
	SiO2-PW	35.933	2.325	0.144	12.7%
	% Diatom	**58.880**	**4.199**	**0.050**	**20.8%**

1003

1004

Table S2. Non-parametric multiple regression results using the DistLM routine on the overall variability of MPB metabolic rates and biomass (P_N, R_D and Chla) as a function of environmental variables using the Best selection procedure and the second order Akaike's information criterion (AICc). Results for up to three explanatory variables and the overall three best solutions independently of number of variables with the smallest value of AICc are shown. R^2: percentage of variance explained by the model. RSS: residual sum of squares.

Best result for each number of variables					
	AICc	**R^2**	**RSS**	**Variables numbers**	**Selection**
P_N	9.814	0.414	23.782	1	SL
	10.588	0.480	21.116	2	SL, NH4-PW
	11.473	0.547	18.401	3	SL, NO3-PW, PO4-PW
R_D	-28.667	0.406	2.804	1	SL
	-27.822	0.470	2.500	2	Dist, SL
	-28.524	0.577	1.994	3	% mud, OC, NO3-PW
Chla	45.513	0.390	172.81	1	SL
	42.743	0.555	126.02	2	% mud, PO4-PW
	44.487	0.593	115.18	3	% mud, C:N, PO4-PW

Overall best solutions					
	AICc	**R^2**	**RSS**	**Variables numbers**	**Selection**

P_N	9.814	0.414	23.782	1	SL
	10.588	0.480	21.116	2	SL, NH_4-PW
	11.473	0.547	18.401	3	SL, NO_3-PW, PO_4-PW
R_D	-28.667	0.406	2.804	1	SL
	-28.524	0.577	1.994	3	% mud, OC, NO3-PW
	-27.822	0.470	2.500	2	Dist, SL
Chl-a	42.743	0.555	126.02	2	% mud, PO_4-PW
	44.487	0.593	115.18	3	% mud, C:N, PO_4-PW
	45.436	0.571	121.42	3	% mud, C:N, NO_3-PW